5-15-2009

Ground Target Tracking with Multi-Lane Constraint

Yangsheng Chen
University of New Orleans

Ground Target Tracking with Multi-Lane Constraint

A Thesis

submitted to the Graduate Faculty of the
University of New Orleans
in partial fulfillment of the
requirements for the degree of

Master of Science
in
The Department of Electrical Engineering

by
Yangsheng Chen
B.S., Changsha Institute of Technology, 2003
May, 2009

Acknowledgements

The author would like to sincerely thank Dr. X.Rong Li and Dr. Vesselin Jilkov for their guidance, support and encouragement throughout my graduate program in the Department of Electrical Engineering at University of New Orleans. I would like to give my thanks to my graduate committee member Dr. Huimin Chen for his good suggestions and comments on my thesis.

TABLE OF CONTENTS

LIST OF TABLES

LIST OF FIGURES

ABSTRACT

Knowledge of the lane that a target is located in is of particular interest in on-road surveillance and target tracking systems. We formulate the problem and propos two approaches for on-road target estimation with lane tracking. The first approach for lane tracking is lane identification based on a Hidden Markov Model (HMM) framework. Two identifiers are developed according to different optimality goals of identification, i.e., the optimality for the whole lane sequence and the optimality of the current lane where the target is given the whole observation sequence. The second approach is on-road target tracking with lane estimation. We propose a 2D road representation which additionally allows to model the lateral motion of the target. For fusion of the radar and image sensor based measurement data we develop three, IMM-based, estimators that use different fusion schemes: centralized, distributed, and sequential. Simulation results show that the proposed two methods have new capabilities and achieve improved estimation accuracy for on-road target tracking.

Key Words: Ground Target Tracking, HMM, Lane Identifier, 2D Road Coordinates, IMM, Lane Estimator, Sensor Data Fusion

CHAPTER I

INTRODUCTION

In this thesis, we consider two main problems in on-road ground target traking-lane identification/estimation, and precision 2 dimensional (2D) tracking based on fusion of radar and image sensor based measurements. In the project of on-road target tracking with lane identification and lane estimation, we use the HMM framework to formulate and solve the lane identification problem. The target motion across lanes is modeled in discrete-time through a Markov chain with known initial and transition probabilities. The multiple lanes of the road are the states of this Markov model. It is assumed that direct observations of the lane of a target with some observation probability matrix (OPM) are available. We derive the OPM based on the assumption that an image sensor (e.g., a camera) provides raw observation data in an on-road target motion scenario. The lane tracking is done in terms of both the optimal estimation of the lane sequence and of the current lane of the target, given the observations from the starting time to the current time. We call the first estimator the *lane sequence estimator* (LSE) or *lane sequence identifier* (LSI), and the second one the *lane filter* (LF) or *lane identifier* (LI). Performance evaluation of both estimators is done by Monte Carlo simulations. The estimators assume knowledge of the transition probability matrix (TPM) of the motion model. Since in practice it is hard to come by with an accurate value of this TPM, we also study the performance of the LSE and LF under mismatch between the TPM used by the estimators and the true TPM (used for ground truth generation) [1].

In the project of precision tracking/fusion, we first propose a 2D road representation which allows to model the lateral motion of the target (the motion along the direction transversal to the road) by accounting for the vehicle displacement from the road axis [2]. Based on this representation we describe the target longitudinal and lateral maneuvering

behavior in 2D road coordinates using multiple models. Additionally, for describing longitudinal maneuver modes of motion we utilize an improved, mean-adaptive acceleration, model proposed originally in [3]. It is assumed that radar (e.g., ground moving target indicator (GMTI)) and image sensor based measurements are available for the purpose of tracking. For fusion of the radar and image sensor based measurement data we develop three, IMM-based, estimators that use different fusion schemes: centralized, distributed, and sequential. The centralized estimator (CE) processes all data jointly. The distributed estimator (DE) uses radar based and image sensor based local estimates to provide a global estimate of the target displacement from the road axis. The sequential estimator (SE) first obtains an estimate of the target displacement based on the image sensor measurement, and then feeds it into the radar based estimator to obtain an estimate of the longitudinal motion (mileage) target state.

The remaining part of this thesis is organized as follows. Chapter 2 presents a literature survey of on-road target tracking. Chapter 3 describes the proposed lane identifiers, and their performance evaluation. Chapter 4 presents the algorithm development and Monte Carlo simulation results of on-road target tracking using radar and image sensor based measurement. Finally, Chapter 5 provides conclusions.

CHAPTER II

LITERATURE SURVEY OF ON-ROAD TARGET TRACKING

Surveillance of ground targets, including tracking of on-road targets, is important for many civilian and military applications. A great deal of research in this area has been done in the recent years, e.g., [1, 4, 5, 6, 7, 8, 9, 10, 11, 12, 13, 14]. Ground target tracking with road network information is much more difficult than tracking an aerial targets, due to the highly nonlinear constraints on the target's motion, the traffic density, the terrain observability, the large number of false alarm, and so on. The central issue in tracking a target moving on a road is to find good ways to account for the road network information.

The first problem is how to model targets traveling along a road. Targets traveling on a road maintain nearly costant velocity for most of the time, while the target may slow down when it is close to an intersection of the road, makes sharp turn or goes up-hill, and it may speed up when it leaves the intersection or goes down-hill.

The second problem is how to use the information of the road network. This is one of the most difficult problem for on-road target tracking, because of its high nonlinearity of the road network. There are four categories of techniques to make use of the road network information in target estimation [11]. The first class is the post-processing correction technique, which does a correction uses traditional state estimation methods and move the estimation on the road so that it is under the road network constraint [15]. The second class uses the road information as the pseudo measurements. A pseudo measurement is the constrained velocity vector by the direction of a road segment [8]. The third class is to incorporate the road network into the tracking algorithm. There are two typical approaches for the third class of methods. The first approach is that target motion is modeled adaptively by tuning the covariance of the process noise according to the road information, but it can not guarantee the target estimation always be on the road [16] [17]. The second approach

in this class is to treat the problem as constrained estimation with road network, which is highly nonlinear [18]. The fourth class of using road network information is to represent the road network as one dimension as (1D), so that the target motion model is just in one dimension. 1D representation of road reduces the target motion model significantly, but the measurement equations become highly nonlinear. This approach can easily model target interactions with the road network and with other targets at intersections for instance. The 1D road representation achieves good performance comparing with other approaches [11, 12].

Most often on-road target dynamics are modeled in Cartesian coordinates based on traditional motion models, such as the constant velocity (CV), constant acceleration (CA), Singer model, etc., and additional means are used to constrain the target motion to the road. However, it is more natural and convenient to model the target motion directly in road coordinates. A one dimensional (1D) representation of a road network was introduced in [11] and the target motion on a road was described in terms of traveled distance (mileage) coordinate. The same approach was also used in [12]. The 1D model is very convenient for describing the longitudinal target motion (the motion along the direction of the road) since it simplifies the kinematics considerably. However, it ignores the width of the road which can lead to yielding significant biases of the target state estimates when the road width is large, e.g., the road has multiple lanes. To overcome this deficiency we propose in [2] a 2D road representation which additionally allows to model the lateral motion of the target (the motion along the direction transversal to the road) by accounting for the vehicle displacement from the road axis. This type of approach of lane tracking is lane estimation which estimates the lateral location of the target (the location along the direction transversal to the road).

Lane tracking of on-road target is a new problem that attracted our interest—we have not found any paper published on this problem. Knowing the lane that a target is located in is of particular interest in on-road surveillance and target tracking systems. In addition, if a good estimate of the lane that a target is located in is available it could help improve the estimate of the location and motion of the target.

We proposed in [1] the HMM framework to formulate and solve the lane identification problem. The Hidden Markov Model (HMM) has been heavily researched and used over the past several decades [19, 20, 21, 22, 23], and successfully applied to a wide variety of applications, especially in the speech recognition area [24, 25, 26]. HMM is usually used to solve three problems. The first problem is that given the model $\lambda = (A, B, \pi)$, how to computer $P(O|\lambda)$, the probability of occurrence of the observation sequence $O = O_1, O_2, ..., O_T$; The second problem is that given the model $\lambda = (A, B, \pi)$, how to choose the state sequence $I = i_1, i_2, ..., i_T$, so that the joint probility of the state sequence I and observation sequence $O = O_1, O_2, ..., O_T$ is maximized, e.g., maximizing $P(O, I|\lambda)$. The third problem is how to adjust the parameters $\lambda = (A, B, \pi)$, so that $P(O|\lambda)$ or $P(O, I|\lambda)$ is maximized. For our problem of lane identification, we proposed to solve the problem which is to maximize the joint probability of the current state i_T and the observation sequence $O = O_1, O_2, ..., O_T$, e.g., maximizing $P(O, i_T|\lambda)$.

CHAPTER III

LANE IDENTIFICATION

3.1 Problem Formulation and Lane Estimation

3.1.1 Target Motion Model

It is assumed that a target is moving on a road with N lanes. The target motion across lanes is modeled by a Markov chain $\{l_t\}_{t=1,2,...}$ as follows.

Let $l_t \in \{1, 2, \ \ldots, \ N\}$ denote the lane in which the target is at discrete time $t = 1, 2, \ \ldots, \ T$. The initial probability vector and the *transition probability matrix* (TPM) of the chain are $\boldsymbol{\pi} = \{\pi_i\}_{i=1}^{N}$ and $A = \{a_{ij}\}_{i,j=1}^{N}$, respectively. In the context of motion across lanes $\pi_i = P(l_1 = i)$ denotes the *a priori* probability of the target being in lane i at the beginning (at time $t = 1$) and $a_{ij} = P(l_{t+1} = j | l_t = i)$ denotes the probability of the target being in lane j at time $t + 1$ given that it was in lane i at time t. We assume that the TPM A is time invariant.

3.1.2 Observation Model

It is assumed that direct observations of the lane of a target are available. An observation, $O_t = O_t(i)$, denotes that the target is declared by the sensor to be in lane i at time t. The observation mechanism is statistically modeled by an *observation probability matrix* (OPM) $B = \{b_j\left(O_t(i)\right)\}_{j,i=1}^{N}$ where $b_j\left(O_t(i)\right) = P\left(O_t\left(i\right) | l_t = j\right)$ is the probability of observing the target in lane i given that the target is in lane j at time t. We assume that the OPM B is time invariant.

3.1.3 Lane Sequence Estimator

Given an HMM model $\lambda = (A, B, \boldsymbol{\pi})$ and an observation sequence $O = \{O_1, O_2, ..., O_T\}$ we aim at choosing a lane sequence $L = l_1, l_2, ..., l_T$ so that the joint probability $P(O, L|\lambda)$ is

maximized.[1]

Since

$$P(O|L) = b_{l_1}(O_1)\, b_{l_2}(O_2) ... b_{l_T}(O_T) \tag{1}$$

and

$$P(L) = \pi_{l_1} a_{l_1 l_2} ... a_{l_{T-1} l_T} \tag{2}$$

we have

$$\begin{aligned} P(O,L) &= P(O|L)P(L) \\ &= \pi_{l_1} b_{l_1}(O_1)\, a_{l_1 l_2} b_{l_2}(O_2) ... a_{l_{T-1} l_T} b_{l_T}(O_T) \end{aligned} \tag{3}$$

After defining the weight

$$U(l_1, l_2, ..., l_T) = -\left[\ln\left(\pi_{l_1} b_{l_1}(O_1)\right) + \sum_{t=2}^{T} \ln\left(a_{l_{t-1} l_t} b_{l_t}(O_t)\right)\right] \tag{4}$$

it can be obtained that

$$P(O,L) = \exp\left[-U(l_1, l_2, ..., l_T)\right] \tag{5}$$

The optimal lane sequence estimation is to find

$$(l_1^*, l_2^*, ..., l_T^*) = \arg \max_{\{l_t\}_{t=1}^T} \left[P(O, l_1, l_2, ..., l_T)\right] \tag{6}$$

which is equivalent to

$$(l_1^*, l_2^*, ..., l_T^*) = \arg \min_{\{l_t\}_{t=1}^T} \left[U(l_1, l_2, ..., l_T)\right] \tag{7}$$

Finding the optimal lane sequence is done through the well known Viterbi algorithm given below. The term $-\ln\left(a_{l_{t-1} l_t} b_{l_t}(O_t)\right)$ is the weight associated with the transition $l_{t-1} \to l_t$.

Viterbi LSE algorithm

For $T = 1, 2, \ldots$ recursively compute the optimal lane sequence:

1. Initialization:

[1] The conditioning on λ, common in the HMM literature, is dropped in the sequel to simplify the notation.

For $1 \leq i \leq N$,

$$\delta_1(i) = -\ln(\pi_{l_1}) - \ln(b_{l_1}(O_1)) \tag{8}$$

$$\varphi_1(i) = 0 \tag{9}$$

2. Recursive Computation:

For $2 \leq t \leq T$, and $1 \leq j \leq N$

$$\delta_t(j) = \min_{1 \leq i \leq N} [\delta_{t-1}(i) - \ln(a_{ij})] - \ln(b_j(O_t)) \tag{10}$$

$$\varphi_t(i) = \arg \min_{1 \leq i \leq N} [\delta_{t-1}(i) - \ln(a_{ij})] \tag{11}$$

3. Termination:

$$W_{\min} = \min_{1 \leq i \leq N} \delta_T(i) \tag{12}$$

$$l_T^* = \arg \min_{1 \leq i \leq N} \delta_T(i) \tag{13}$$

4. Tracking back the optimal lane sequence:

For $t = T-1, T-2, ..., 1$,

$$l_t^* = \varphi_{t+1}(l_{t+1}^*). \tag{14}$$

It can be easily seen that $L_T^* = \{l_1^*, l_2^*, ..., l_T^*\}$ is the optimal lane sequence from time $t = 1$ to time $t = T$.

3.1.4 Lane Filter

The variable $\alpha_T(i)$ is defined as

$$\alpha_T(i) = P(O_1, O_2, ..., O_T, l_T = i) \tag{15}$$

By Bayes' rule the probability of the target being in lane i at time t given the observation sequence $O = O_1, O_2, ..., O_T$ is

$$P(l_T = i|O) = \frac{P(l_T = i, O)}{P(O)} = \frac{\alpha_T(i)}{P(O)} \tag{16}$$

Further, we have subsequently

$$\begin{aligned}
\alpha_{T+1}(j) &= P(O_1, O_2, ..., O_T, O_{T+1}, l_{T+1} = j) \\
&= \sum_{i=1}^{N} [P(O_{T+1}, l_{T+1} = j | O_1, O_2, ..., O_T, l_T = i) \\
&\qquad \cdot P(O_1, O_2, ..., O_T, l_T = i)] \\
&= \sum_{i=1}^{N} [P(O_{T+1} | O_1, O_2, ..., O_T, l_T = i, l_{T+1} = j) \\
&\qquad \cdot P(l_{T+1} = j | O_1, O_2, ..., O_T, l_T = i) \alpha_T(i)] \\
&= \sum_{i=1}^{N} [P(O_{T+1} | l_{T+1} = j) P(l_{T+1} = j | l_T = i) \alpha_T(i)] \\
&= \sum_{i=1}^{N} [P(O_{T+1} | l_{T+1} = j) a_{ij} \alpha_T(i)] \\
&= b_j(O_{T+1}) \sum_{i=1}^{N} a_{ij} \alpha_T(i) \qquad (17)
\end{aligned}$$

The probability of the observation sequence $O = \{O_1, O_2, ..., O_T\}$ is

$$\begin{aligned}
P(O) &= \sum_{i=1}^{N} P(O, l_T = i) \\
&= \sum_{i=1}^{N} \alpha_T(i) \qquad (18)
\end{aligned}$$

The algorithm of optimal estimation of the lane at the current time which we call the lane filter is given as follows.

LF algorithm

Recursively compute the optimal lane estimation at time T for $T = 1, 2, \ldots$:

1. Initialization:

$$\alpha_1(i) = \pi_i b_i(O_1), 1 \leq i \leq N \qquad (19)$$

2. Recursion:

For $t = 1, 2, ..., T-1, 1 \leq j \leq N$,

$$\alpha_{t+1}(j) = b_j(O_{t+1}) \sum_{i=1}^{N} [a_{ij} \alpha_t(i)] \qquad (20)$$

3. Observation sequence probability:

$$P(O) = \sum_{i=1}^{N} \alpha_T(i) \qquad (21)$$

4. Optimal estimate of the lane at current time T

$$\begin{aligned} l_T^* &= \arg \max_{1 \le i \le N} P(l_T = i, O) \\ &= \arg \max_{1 \le i \le N} \frac{\alpha_T(i)}{P(O)} \end{aligned} \tag{22}$$

The sequence $L_T^* = \{l_1^*, l_2^*, ..., l_T^*\}$ is the estimation result we obtain at times $T = 1, 2, \ldots$

3.2 Observation Probability Matrix

Here we propose a method for deriving the observation probability matrix B for a particular scenario.

It is assumed that a signal processor can provide the displacement d of the target center from the left edge of the road. For example, if a surveillance system uses raw image data (provided, e.g., by a camera on a satellite), a measurement $z = d + v$ of this displacement can be extracted by using image processing techniques. We assume that the measurement error v is zero-mean with Gaussian distribution, truncated outside the road. Then

$$z \sim f(z) = \begin{cases} \frac{1}{c}\mathcal{N}(z; d, \sigma_v^2) & \text{if } 0 < z < 2N\Delta \\ 0 & \text{otherwise} \end{cases} \tag{23}$$

where N is the number of lanes, 2Δ is the width of each lane, $c = \Phi\left(\frac{2N\Delta - d}{\sigma_v}\right) - \Phi\left(\frac{-d}{\sigma_v}\right)$ is a normalization constant, and $\Phi(\cdot)$ denotes the standard Gaussian cumulative distribution function (cdf).

When a target is in a lane we assume that the central point of the vehicle is on the central line of this lane. Given that a target is in lane j, the probability density function $f_j(z)$ of a measurement originating from the target is (Fig.1)

$$f_j(z) = \begin{cases} \frac{1}{c_j}\mathcal{N}(z; (2j-1)\Delta, \sigma_v^2) & \text{if } 0 < z < 2N\Delta \\ 0 & \text{otherwise} \end{cases} \tag{24}$$

where

$$c_j = \Phi\left(\frac{(2(N-j)+1)\Delta}{\sigma_v}\right) - \Phi\left(\frac{-(2j-1)\Delta}{\sigma_v}\right) \tag{25}$$

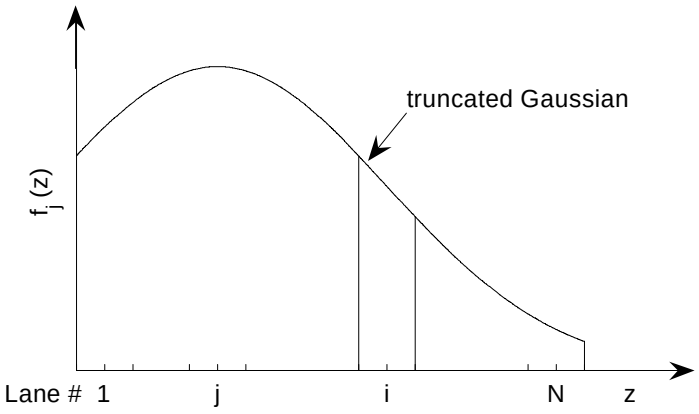

Figure 1: Measurement PDF

Then, after some straightforward calculation, we have the final result

$$\begin{aligned} P \quad (O_t(i)|l_t = \quad j) & \qquad (26) \\ = \qquad P\left(2(i-1)\Delta < z < 2i\Delta\right) & \qquad (27) \\ = \qquad \frac{1}{c_j}\left[\Phi\left(\frac{(2(i-j)+1)\Delta}{\sigma_v}\right) - \Phi\left(\frac{(2(i-j)-1)\Delta}{\sigma_v}\right)\right] & \qquad (28) \end{aligned}$$

Clearly, the idea of the above derivation is not limited to Gaussian distribution of the error at the output of the image processing.

For $N = 3$, $\Delta = 2$ m and $\sigma_v = 2$ m we obtained that

$$\begin{aligned} B \quad &= \quad \left\{b_j\left(O_t(i)\right)\right\}_{j,i=1}^{3} \\ &= \quad \begin{bmatrix} 0.8114 & 0.1870 & 0.0016 \\ 0.1577 & 0.6845 & 0.1577 \\ 0.0016 & 0.1870 & 0.8114 \end{bmatrix} \end{aligned} \qquad (29)$$

This OPM was used in the simulations described next.

3.3 Simulation and Performance Evaluation

3.3.1 Performance Measures

In the simulation we applied the following measures for performance evaluation.

Probability of being in the correct lane at the current time

$$P_T = \frac{1}{N_r}\sum_{r=1}^{N_r} S_T^r \qquad (30)$$

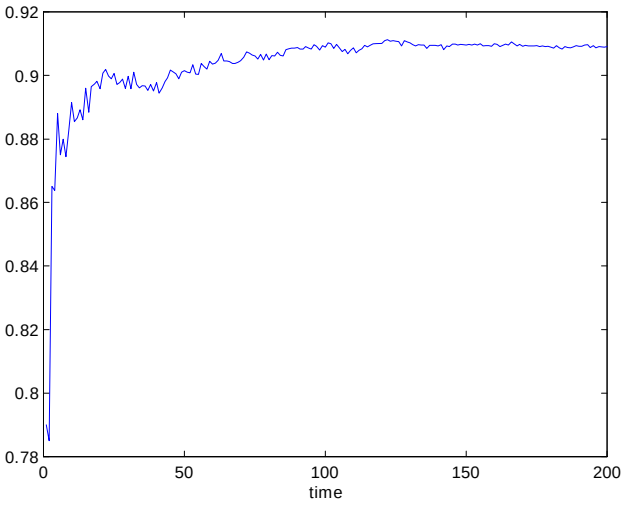

Figure 2: Average probability of being correct of LSE. 200 runs.

where $S_T^r = 1$ or 0. $S_T^r = 1$ when the lane identified at the current time T is correct, and $S_T^r = 0$ otherwise. N_r is the number of runs.

Time-average probability of being in the correct lane

$$P_{ac} = \frac{1}{N_r} \sum_{r=1}^{N_r} P_c^r \tag{31}$$

where for each single run r

$$P_c^r = \frac{k}{n} \tag{32}$$

is the percentage of times the identified lane is correct and n is the number of observations in this run.

Error probability matrix.

It is calculated via normalization of the confusion matrix, i.e.,

$$C = \left(\frac{c_{ij}}{\sum_{i=1}^{N} c_{ij}} \right)_{i,j=1}^{N} \tag{33}$$

where c_{ij} is the number of times that the target is declared in lane i while it is actually in lane j.

3.3.2 Simulation

The parameters of the ground truth are as follows.

$N = 3$. Initial lane probabilities

$$\pi = \begin{bmatrix} 0.3 & 0.4 & 0.3 \end{bmatrix}.$$

Lane transition probability matrix

$$A = \{a_{ij}\} = \begin{bmatrix} 0.92 & 0.07 & 0.01 \\ 0.04 & 0.92 & 0.04 \\ 0.01 & 0.07 & 0.92 \end{bmatrix}$$

The observation probability matrix B in this case is given by (29), as derived in Sect. III.

The performances of the LSE and LF are illustrated in Figures 2 and 3, respectively. From Figure 2 we can see that the LSE provides good performance. After about 50 time steps the probability of being correct on the lane sequence is around 0.92 and it tends to increase as time goes. From Figure 3, we can also see good performance using the LF algorithm. Note that the performance measures used in Figure 2 and Figure 3 are different: The first one is the average probability of being correct on the lane sequence from time 1 to the current time; The second one is the probability of being correct on the lane at the current time over all the runs.

The error probability matrix of the LSE at T = 200 is

$$C = \begin{bmatrix} 0.8600 & 0.1400 & 0 \\ 0.0485 & 0.8738 & 0.0777 \\ 0 & 0.1702 & 0.8298 \end{bmatrix}.$$

For the LF at T = 200 it is

$$C = \begin{bmatrix} 0.8800 & 0.1200 & 0 \\ 0.0388 & 0.8932 & 0.0680 \\ 0 & 0.1702 & 0.8298 \end{bmatrix}.$$

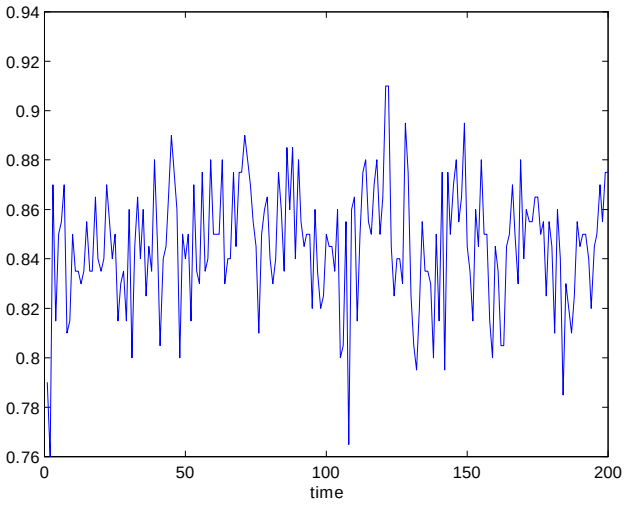

Figure 3: Probability of being correct of LF. 200 runs.

Comparing these error probability matrices we see that, as it should be, the LF has better performance concerning the lane at the current time than LSE.

3.3.3 Unknown Lane TPM

In order to see the effect of mismatch between the true TPM used in the simulation and the one used by the estimators, we analyze the sensitivity of the elements of the TPM using a 3 by 3 matrix defined as

$$\Delta = (\Delta a_{ij}) = (a_{ij}) - \left(a_{ij}^{v}\right), 1 \leq i, j \leq 3$$

where $A = \{a_{ij}\}_{1 \leq i,j \leq 3}$ is the ground truth, and $A_v = \left\{a_{ij}^{v}\right\}_{1 \leq i,j \leq 3}$ is the transition matrix used by the HMM estimators. A is chosen as the matrix A defined in Sect. IV B. Due to the symmetry of the TPM we analyze the sensitivity of the elements a_{11}, a_{12}, a_{22}.

First, we analyze the effect of a_{11} on the performance of LSE and LF by comparing the performance of four cases given in Table 1.

Secondly, we analyze the effect of a_{12} of four cases given in Table 2.

Thirdly, we analyze the effect of a_{11} with respect to a_{12} on the performance of LSE and LF by comparing the performance of four cases given in Table 3.

Case 1:	Case 2:
$\Delta_1 = \begin{bmatrix} 0 & 0 & 0 \\ 0 & 0 & 0 \\ 0 & 0 & 0 \end{bmatrix}$	$\Delta_1 = \begin{bmatrix} .1 & 0 & -.1 \\ 0 & 0 & 0 \\ 0 & 0 & 0 \end{bmatrix}$
Case 3:	Case 4:
$\Delta_1 = \begin{bmatrix} .2 & 0 & -.2 \\ 0 & 0 & 0 \\ 0 & 0 & 0 \end{bmatrix}$	$\Delta_1 = \begin{bmatrix} .4 & 0 & -.4 \\ 0 & 0 & 0 \\ 0 & 0 & 0 \end{bmatrix}$.

Table 1: TPM mismach analysis of a_{11}

Case 1:	Case 2:
$\Delta_2 = \begin{bmatrix} 0 & 0 & 0 \\ 0 & 0 & 0 \\ 0 & 0 & 0 \end{bmatrix}$	$\Delta_2 = \begin{bmatrix} 0 & .03 & -.03 \\ 0 & 0 & 0 \\ 0 & 0 & 0 \end{bmatrix}$
Case 3:	
$\Delta_2 = \begin{bmatrix} 0 & .06 & -.06 \\ 0 & 0 & 0 \\ 0 & 0 & 0 \end{bmatrix}$	

Table 2: TPM mismach analysis of a_{12}

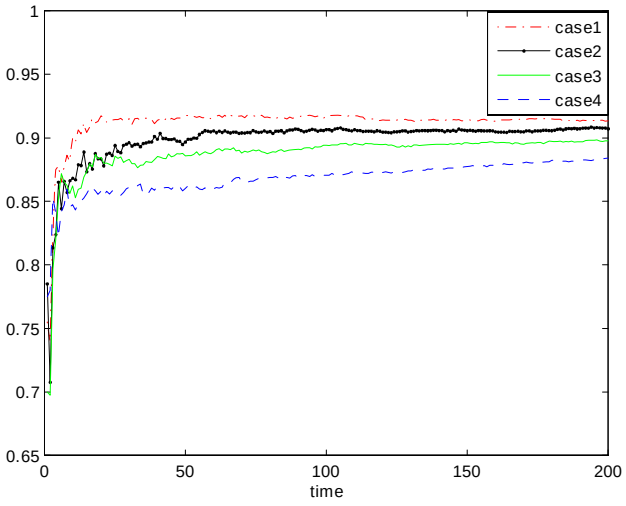

Figure 4: Average probability of being correct of LSE for $\triangle_1$.200 runs.

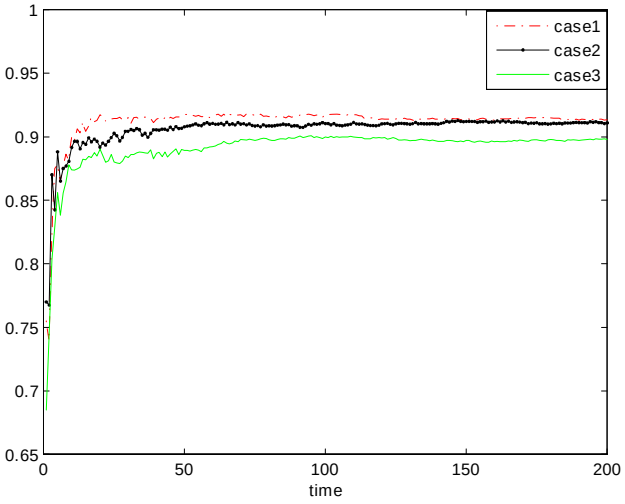

Figure 5: Average probability of being correct of LSE for $\triangle_2$.200 runs.

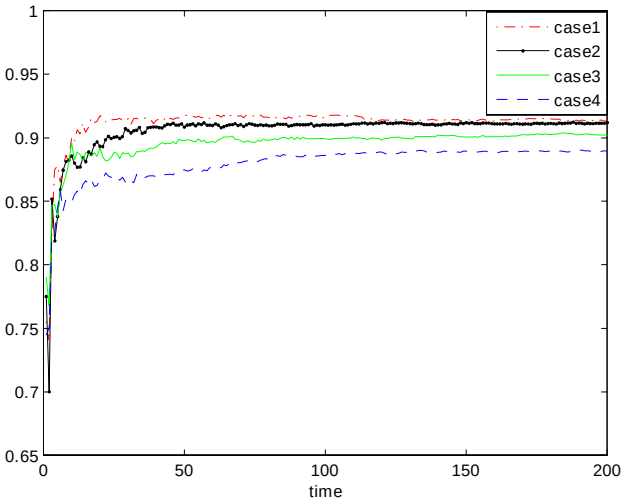

Figure 6: Average probability of being correct of LSE for $\triangle_3$.200 runs.

Case 1:	Case 2:
$\Delta_3 = \begin{bmatrix} 0 & 0 & 0 \\ 0 & 0 & 0 \\ 0 & 0 & 0 \end{bmatrix}$	$\Delta_3 = \begin{bmatrix} .1 & -.1 & 0 \\ 0 & 0 & 0 \\ 0 & 0 & 0 \end{bmatrix}$
Case 3:	Case 4:
$\Delta_3 = \begin{bmatrix} .2 & -.2 & 0 \\ 0 & 0 & 0 \\ 0 & 0 & 0 \end{bmatrix}$	$\Delta_3 = \begin{bmatrix} .4 & -.4 & 0 \\ 0 & 0 & 0 \\ 0 & 0 & 0 \end{bmatrix}$.

Table 3: TPM mismach analysis of a_{11} with respect to a_{12}

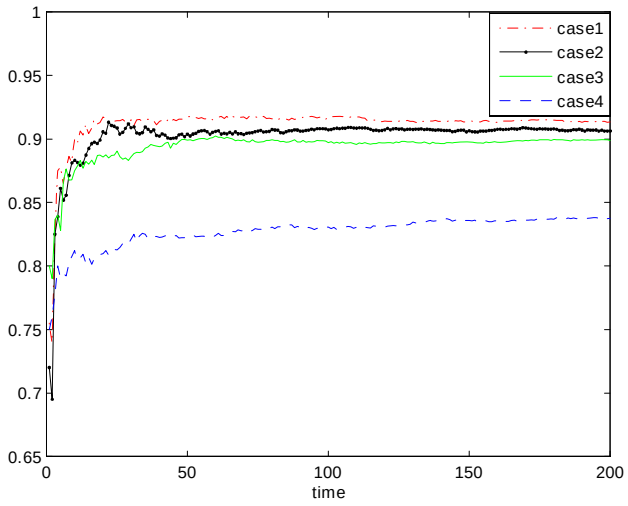

Figure 7: Average probability of being correct of LSE for $\triangle_4$.200 runs.

Case 1:	Case 2:
$\Delta_4 = \begin{bmatrix} 0 & 0 & 0 \\ 0 & 0 & 0 \\ 0 & 0 & 0 \end{bmatrix}$	$\Delta_4 = \begin{bmatrix} 0 & 0 & 0 \\ -.05 & 0.1 & -.05 \\ 0 & 0 & 0 \end{bmatrix}$
Case 3:	Case 4:
$\Delta_4 = \begin{bmatrix} 0 & 0 & 0 \\ -.1 & .2 & -.1 \\ 0 & 0 & 0 \end{bmatrix}$	$\Delta_4 = \begin{bmatrix} 0 & 0 & 0 \\ -.2 & .4 & -.2 \\ 0 & 0 & 0 \end{bmatrix}$.

Table 4: TPM mismach analysis of the effect of a_{22}

Lastly, we analyze the effect of a_{22} of four cases given in Table 4.

Figure 4 - 7 shows the performance of the LSE with different TPMs A_v. It is seen from Figure 4, 5, and 6 that Δa_{11} and Δa_{12} have some effect on the performance of the LSE, but not very significant. From Figure 7 we can see that the performance of LSE is affected by a_{22} very strongly. Figure 8 - 11 shows similar results for the LF. It seems that the element a_{22} of TPM has much greater impact on the performance. If the ground truth, especially the true a_{22} of TPM, is unknown, the choice of lane TPM will affect the lane tracking performance heavily. How to identify the lane transition probability matrix appears to be an important problem that we intend to address in the future.

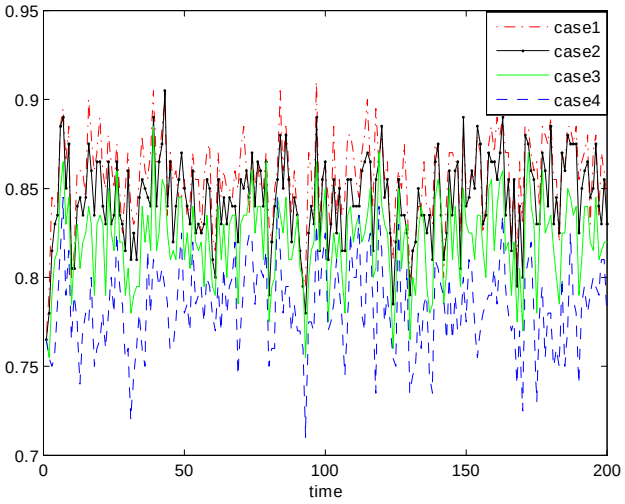

Figure 8: Probability of being correct of LF for $\triangle_1$. 200 runs.

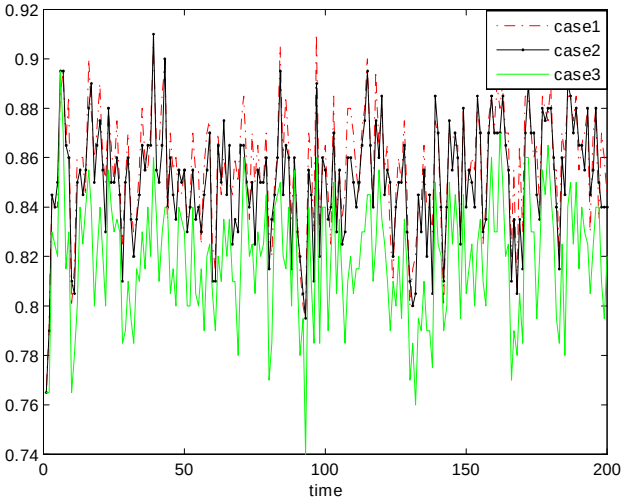

Figure 9: Probability of being correct of LF for $\triangle_2$. 200 runs.

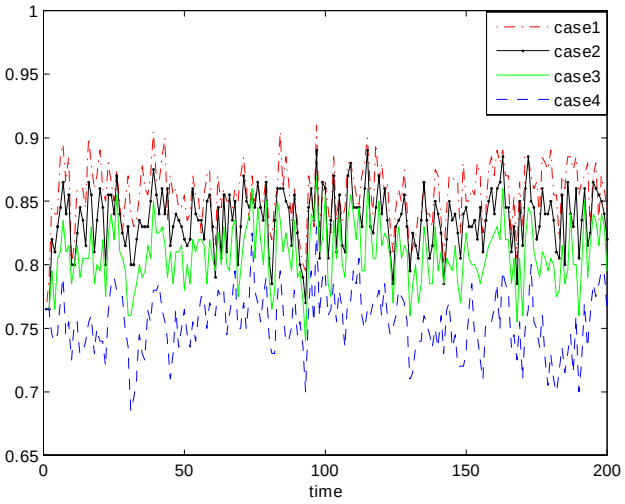

Figure 10: Probability of being correct of LF for $\triangle_3$. 200 runs.

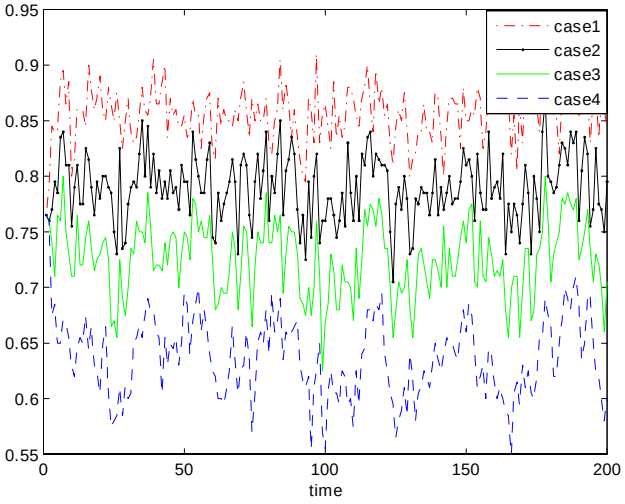

Figure 11: Probability of being correct of LF for $\triangle_4$. 200 runs.

CHAPTER IV

ON-ROAD TARGET TRACKING USING RADAR AND IMAGE SENSOR BASED MEASUREMENTS

4.1 2D Road Coordinates Representation

A 1D representation of a road network was introduced in [11]. This 1D model is very convenient for describing the *longitudinal motion*[1] of an on-road vehicle since it simplifies the kinematics considerably. However, it ignores the width of the road which can lead to yielding significant biases of the target state estimates when the road width is large, e.g., the road has multiple lanes. To overcome this deficiency we propose a 2D road representation which additionally allows to model the *lateral motion*[2] of the target by accounting for the vehicle displacement from the road axis. The 2D road – vehicle geometry is illustrated in Fig.12

A segment of a road is represented by the curve of its axis (center line) and by its width. With respect to a global Cartesian coordinate system Oxy the axis curve $\mathcal{C}$ is assumed known, e.g., given in *natural parametric form* [27] by

$$\mathcal{C}: \begin{cases} x_c = x_c(s) \\ y_c = y_c(s), \end{cases} \qquad 0 \le s \le s_f \tag{34}$$

where $x_c(s)$ and $y_c(s)$ are known functions of the natural parameter—the arc length s. It is assumed that the road segment under consideration has N lanes and the width of each one is Δ.

A point $V = (x, y)$ on the road (the location of a vehicle center) can be represented as $V = (s, d)$ where d is the signed displacement of V from the center line $\mathcal{C}$ (the signed distance between the orthogonal projection C of V onto $\mathcal{C}$)[3], and s is the curve length of

[1] The motion along the direction the road.

[2] The motion along the direction transversal to the road.

[3] $d > 0$ if V is to right-hand side of the axis curve C_0C_f and $d < 0$ if V is to left-hand side of the axis curve C_0C_f .

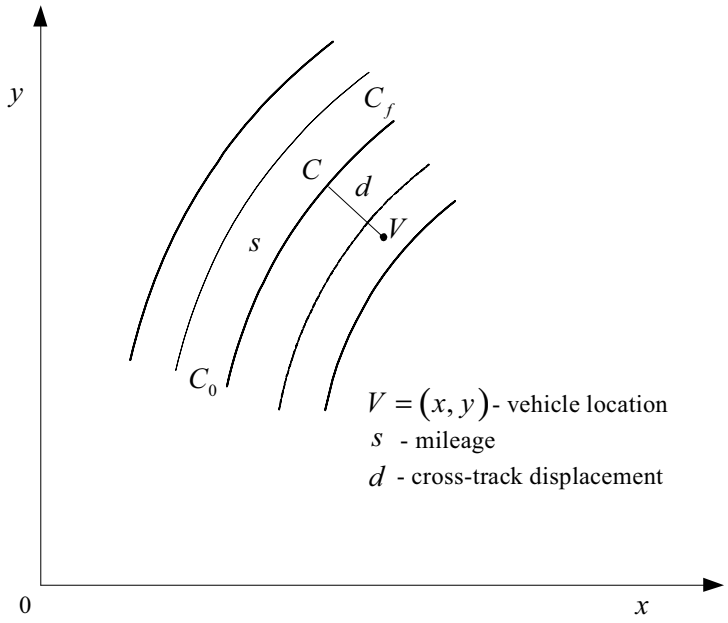

Figure 12: Road – Vehicle Geometry

the center line segment from the known segment initial point $C_0 = (x_c(0), y_c(0))$ and the projection point $C = (x_c(s), y_c(s))$ (Fig.12). Vice versa, given s, point $C = (x_c(s), y_c(s))$ is uniquely determined through (34). Furthermore, given point C and displacement d, point V is uniquely determined on the road since the road width $N\Delta$ is much smaller than the radius of curvature of $\mathcal{C}$. The displacement is actually subject to the constraint $|d| \leq w = N\Delta/2 - \delta$, where δ is an offset determined, e.g., by (half) of the vehicle width. Thus each point $V = (x, y)$ on the road can be represented in *road coordinates* s and d as $V = (s, d)$, where s is referred to as the *mileage* coordinate and d is referred to as the *displacement* coordinate. Formally, we can write

$$\begin{aligned} x &= g_x(s, d) \\ y &= g_y(s, d) \end{aligned} \qquad 0 \leq s \leq s_f, \;\; -w \leq d \leq w$$

where the mapping $g = (g_x, g_y)$ is the transformation from road coordinates to Cartesian coordinates. In general, obtaining g may not be easy for curve segments with arbitrary shapes. However, most often a road can be approximated with a sufficient accuracy through straight line segments and circular arc segments. Next we determine the road-to-Cartesian coordinate transformation g for linear and circular road segments. It is assumed in the

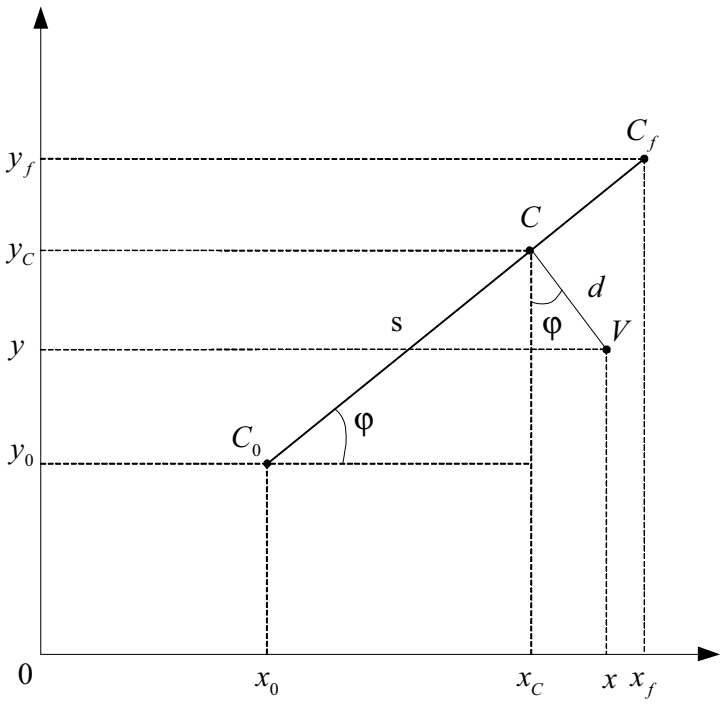

Figure 13: Linear Road Segment

sequel that the width of the road within a segment is constant.

4.1.1 Linear Segment

The geometry of the target on a linear road segment C_0C_f is shown in Fig.13. Let

$$\varphi = \tan^{-1} \frac{y_f - y_0}{x_f - x_0} \tag{35}$$

and consider the case $0 \leq \varphi < \pi/2$. The other three cases for φ: $\pi/2 \leq \varphi < \pi$, $\pi \leq \varphi < 3\pi/2$, and $3\pi/2 \leq \varphi < 2\pi$ can be considered in the same way.

It is easily seen from Fig.13 that

$$\begin{aligned} x &= x_c + \mathrm{sgn}(d) d \sin\varphi \\ y &= y_c - \mathrm{sgn}(d) d \cos\varphi \end{aligned}$$

and

$$\begin{aligned} x_c &= x_0 + s\cos\varphi \\ y_c &= y_0 + s\sin\varphi \end{aligned}$$

Thus

$$x = g_x(s,d) = x_0 + s\cos\varphi + \mathrm{sgn}(d)d\sin\varphi \quad (36)$$

$$y = g_y(s,d) = y_0 + s\sin\varphi - \mathrm{sgn}(d)d\cos\varphi \quad (37)$$

where

$$0 \le s \le s_f, \quad -N\triangle/2 < d < N\triangle/2, \quad (38)$$

4.1.2 Circular Arc Segment

The geometry of the target on a circular arc road segment C_0C_f is shown in Fig.14. The center $M = (x_M, y_M)$, radius R, initial point C_0, and final point C_f are known. Let

$$\psi = \frac{s}{R} \quad (39)$$

$$\psi_0 = \tan^{-1}\frac{y_M - y_0}{x_M - x_0} \quad (40)$$

It is easily seen from Fig.14 that

$$x = g_x(s,d) = x_M - (R-d)\cos(\frac{s}{R} - \psi_0) \quad (41)$$

$$y = g_y(s,d) = y_M + (R-d)\sin(\frac{s}{R} - \psi_0) \quad (42)$$

There are several types of circular arc segment according to the road direction and the orientation of the circular arc. In all cases g can be derived in same way.

4.2 Target Motion Models in Road Coordinates

The main reason of introducing the 2D road coordinates in Sec. 4.1 is that motion of a target on a road is modeled more naturally in road coordinates than in the usual Cartesian coordinates.

4.2.1 Longitudinal Motion

The motion along a given road can be conveniently described by the acceleration $\ddot{s}(t) = a^s(t)$ where $s(t)$ is the road segment arc length (mileage coordinate) at time t. The acceleration function $a^s(t)$ is in general unknown because it depends on largely unknown factors—most

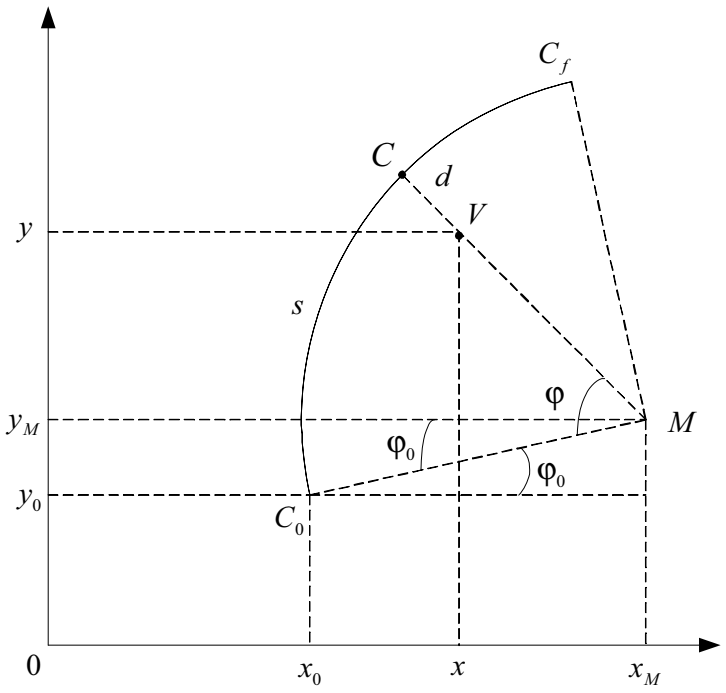

Figure 14: Circular Road Segment

notably, on the vehicle control (driver behavior) and on the vehicle performance characteristics. It is common to model $a^s(t)$ as a random process. The reader is referred to [3] for a comprehensive survey on the available techniques. Below we briefly summarize the models used in this thesis.

With a state vector $x^s = [s, \dot{s}, \ddot{s}]'$ we consider the following generic discrete-time model

$$x^s_{k+1} = Fx^s_k + \Gamma u_k + Gw^s_k \tag{43}$$

where $w^s_k \sim N(0, Q_s)$ is white process noise, and the matrices F and G are defined below to model different modes of motion.

4.2.1.1 Nearly CV Model

The nearly *constant velocity* (CV) model is intended to describe nonmaneuvering mode of motion. The model is given by (43) with $u_k \equiv 0$ and system matrices

$$F_{CV} = \begin{bmatrix} 1 & T & 0 \\ 0 & 1 & 0 \\ 0 & 0 & 0 \end{bmatrix}, \; G_{CV} = \begin{bmatrix} T^2/2 \\ T \\ 0 \end{bmatrix} \tag{44}$$

where T is the sampling interval, and with process noise variance $Q_s = \sigma_s^2 = \sigma_{s_{CV}}^2$.

4.2.1.2 Nearly CA Model

The nearly *constant acceleration* (CV) model is intended to describe maneuvering mode motion with nearly constant acceleration. The model is given by (43) with $u_k \equiv 0$ and system matrices

$$F_{CA} = \begin{bmatrix} 1 & T & T^2/2 \\ 0 & 1 & T \\ 0 & 0 & 1 \end{bmatrix}, \; G_{CA} = \begin{bmatrix} T^2/2 \\ T \\ 1 \end{bmatrix} \tag{45}$$

and process noise variance $Q_s = \sigma_s^2 = \sigma_{s_{CA}}^2$.

4.2.1.3 Mean-Adaptive Acceleration Model

The nearly CA model has very limited capability for describing various maneuvering modes of motion. A better choice is the first-order correlated acceleration model (best known as the Singer model) and, furthermore, its extension known as the "current" model [3]. The *mean-adaptive acceleration* (MAA) model, originally proposed in [3], is an improvement over the "current" model. The MAA model is given by (43) with $u_k \equiv \bar{a}_k$ and system

matrices

$$F_{MAA} = \begin{bmatrix} 1 & T & \left(\alpha T - 1 + e^{-\alpha T}\right)/\alpha^2 \\ 0 & 1 & \left(1 - e^{-\alpha T}\right)/\alpha \\ 0 & 0 & e^{-\alpha T} \end{bmatrix} \tag{46}$$

$$\Gamma_{MAA} = G_{CA} - \begin{bmatrix} \left(\alpha T - 1 + e^{-\alpha T}\right)/\alpha^2 \\ \left(1 - e^{-\alpha T}\right)/\alpha \\ e^{-\alpha T} \end{bmatrix} \tag{47}$$

$$G_{MAA} = I_3 \tag{48}$$

where $\alpha = 1/\tau$ where τ is a maneuver specific time constant.

The process noise covariance $Q_s = E(w_k^s w_k^{s\prime}) = 2\alpha\sigma_k^2 Q$ where $Q = [q_{ij}]_{i,j=1}^3$ is a symmetric matrix with

$$\begin{aligned} q_{11} &= \frac{1 - e^{-2\alpha T} + 2\alpha T + \frac{2\alpha^3 T^3}{3} - 2\alpha^2 T^2 - 4\alpha T e^{-\alpha T}}{2\alpha^5} \\ q_{12} &= \frac{e^{-2\alpha T} + 1 - 2e^{-\alpha T} + 2\alpha T e^{-\alpha T} - 2\alpha T + \alpha^2 T^2}{2\alpha^4} \\ q_{13} &= \frac{1 - e^{-2\alpha T} - 2\alpha T e^{-\alpha T}}{2\alpha^3} \\ q_{22} &= \frac{4e^{-\alpha T} - 3 - e^{-2\alpha T} + 2\alpha T}{2\alpha^3} \\ q_{23} &= \frac{e^{-2\alpha T} + 1 - 2e^{-\alpha T}}{2\alpha^2} \\ q_{33} &= \frac{1 - e^{-2\alpha T}}{2\alpha} \end{aligned}$$

and

$$\sigma_k^2 = \begin{cases} \frac{4-\pi}{\pi}\left(a_{\max}^s - \hat{\ddot{s}}_{k|k}\right) & \text{if} \quad \hat{\ddot{s}}_{k|k} > 0 \\ \frac{4-\pi}{\pi}\left(a_{-\max}^s + \hat{\ddot{s}}_{k|k}\right) & \text{if} \quad \hat{\ddot{s}}_{k|k} < 0 \end{cases} \tag{49}$$

where $\hat{\ddot{s}}_{k|k}$ is the filter estimate and $a_{-\max}^s$, $a_{\max}^s$ are lower and upper bounds of the acceleration $\ddot{s}$, respectively.

The mean acceleration $\bar{a}_{k+1}$ is computed adaptively, before the state prediction step $k \mapsto k+1$, by the following recursion

$$\overline{a}_{k+1} = e^{-\alpha T}\hat{\ddot{s}}_{k|k} + \left(1 - e^{-\alpha T}\right)\overline{a}_k \tag{50}$$

4.2.1.4 Multiple Model

Let M_1^s denotes the nonmaneuver CV model, M_2^s denotes a maneuvering motion model (either CA or MAA), and m_k^s denotes the target model of motion at time k. The target *maneuvering behavior*—model sequence $\{m_k^s\}_{k=0,1,\ldots}$—is assumed to be a homogeneous Markov chain $m_k^s \in \{M_1^s, M_2^s\}$ with transition probabilities

$$P\left\{m_k^s = M_j^s | m_{k-1}^s = M_i^s\right\} = \pi_{ij}^s,\ i,j = 1,2 \tag{51}$$

and initial probabilities $\mu_{0,i}^s = P\left\{m_0^s = M_i^s\right\},\ i = 1,2$. The *transition probability matrix* (TPM) $\Pi^s = [\pi_{ij}]_{i,j=1}^2$ and initial probability vector $\boldsymbol{\mu}_0^s = [\mu_{0,1}^s, \mu_{0,2}^s]'$ are assumed known. In practice they are design parameters. The corresponding *hybrid system* model can be written as follows

$$x_{k+1}^s = F(m_k^s)x_k^s + \Gamma(m_k^s)u_k + G(m_k^s)w_k^s(m_k^s) \tag{52}$$

In the sequel we consider two *multiple model* (MM) configurations to model the along-road maneuver behavior of the target: CV-CA MM—with $M_2^s = CA$ and CV-MAA with $M_2^s = MAA$.

4.2.2 Lateral Motion

Let d_k be the displacement of the target center, as defined in Sec. 4.1, at time k. The target motion across the road is described by the following multiple model

$$d_k = \bar{d}^{(l_k)} + w_k^d \quad k = 0,1,\ldots \tag{53}$$

where $\bar{d}^{(l)} = (2l-1)\Delta/2$ is the displacement of the center of the lth lane, $l = 1,2,\ldots,N$, from the road axis, and $w_k^d \sim \mathcal{N}\left(0, \sigma_{w^d}^2\right)$ is white process noise sequence. The process of changing lanes—sequence $\{l_k\}_{k=0,1,\ldots}$—is modeled as a homogeneous Markov chain with transition probabilities

$$P\left\{l_k = j | l_k = i\right\} = \pi_{ij}^d,\ i,j = 1,\ldots,N \tag{54}$$

and initial probabilities $\mu_{0,i}^d = P\left\{l_0 = i\right\},\ i = 1,\ldots,N$. The TPM $\Pi^d = [\pi_{ij}^d]_{i,j=1}^N$ and initial probability vector $\boldsymbol{\mu}_0^d = [\mu_{0,1}^d, \ldots, \mu_{0,N}^d]'$ are assumed known.

4.2.3 Joint Longitudinal & Lateral Motion

Based on (52) and (53) a hybrid system model for the compound base state vector $x = [x_k^{s\prime}, d_k]'$ is as follows.

$$x_{k+1} = \begin{bmatrix} F(m_k^s) & 0 \\ 0 & 0 \end{bmatrix} x_k + \begin{bmatrix} \Gamma(m_k^s) & 0 \\ 0 & 1 \end{bmatrix} \begin{bmatrix} u_k \\ \bar{d}^{(l_k)} \end{bmatrix} + \begin{bmatrix} G(m_k^s) & 0 \\ 0 & 1 \end{bmatrix} \begin{bmatrix} w_k^s(m_k^s) \\ w_k^d \end{bmatrix} \tag{55}$$

The modal state is $(m_k, l_k) \in \{M_1^s, M_2^s\} \times \{1, 2, \ldots, N\}$. The joint transition probabilities

$$P\{(m_k, l_k) = (j_1, j_2) \,|\, (m_{k-1}, l_{k-1}) = (i_1, i_2)\} \tag{56}$$

for $i_1, j_1 = 1, 2; i_2, j_2 = 1, \ldots, N$, and initial probabilities

$$P\{(m_0, l_0) = (i_1, i_2)\} \quad \text{for } i_1 = 1, 2,\ i_2 = 1, \ldots, N \tag{57}$$

complete the model definition. It should be noted the above hybrid model has a nice capability—to model joint maneuvers, both along-road and across-road, by appropriately designing the joint transition probabilities (56).

4.3 Measurement Models

We consider two types of sensors available: radar and image sensor.

4.3.1 Radar Measurements

A radar, e.g., ground moving target indicator (GMTI), provides measurements of the *range* r and *bearing* b of the target in the global coordinate system Oxy (Fig.4.1). If the vehicle

center in road coordinates is (s, d) then the radar measurement model is given by[4]

$$\begin{aligned}\begin{bmatrix} z_r \\ z_b \end{bmatrix} &= \begin{bmatrix} h_r(g_x(s,d), g_y(s,d)) \\ h_b(g_x(s,d), g_y(s,d)) \end{bmatrix} + \begin{bmatrix} v_r \\ v_b \end{bmatrix} \\ &= \begin{bmatrix} \sqrt{g_x(s,d)^2 + g_y(s,d)^2} \\ \tan^{-1}\left(\frac{g_y(s,d)}{g_x(s,d)}\right) \end{bmatrix} + \begin{bmatrix} v_r \\ v_b \end{bmatrix}\end{aligned} \tag{58}$$

where z_r and z_b denote the range and bearing measurements, respectively; $v_r \sim \mathcal{N}\left(0, \sigma_r^2\right)$, $v_b \sim \mathcal{N}\left(0, \sigma_b^2\right)$ are mutually uncorrelated and white noise measurement error processes; and $(g_x(s,d), g_y(s,d))$ is the (known) road-to-Cartesian coordinate transformation, described in Sec. 4.1.

The partial derivatives associated with this model are as follows

$$h_{11}(s,d) = \frac{g_x(s,d)\frac{\partial g_x(s,d)}{\partial s} + g_y(s,d)\frac{\partial g_y(s,d)}{\partial s}}{\sqrt{g_x(s,d)^2 + g_y(s,d)^2}} \tag{59}$$

$$h_{21}(s,d) = \frac{g_x(s,d)\frac{\partial g_x(s,d)}{\partial s} - g_y(s,d)\frac{\partial g_y(s,d)}{\partial s}}{g_x(s,d)^2 + g_y(s,d)^2} \tag{60}$$

$$h_{14}(s,d) = \frac{g_x(s,d)\frac{\partial g_x(s,d)}{\partial d} + g_y(s,d)\frac{\partial g_y(s,d)}{\partial d}}{\sqrt{g_x(s,d)^2 + g_y(s,d)^2}} \tag{61}$$

$$h_{24}(s,d) = \frac{g_x(s,d)\frac{\partial g_x(s,d)}{\partial d} - g_y(s,d)\frac{\partial g_y(s,d)}{\partial d}}{g_x(s,d)^2 + g_y(s,d)^2} \tag{62}$$

They are needed for the extended Kalman filters developed below.

4.3.2 Image-Based Measurements

It is assumed that a measurement z_d of the *displacement* d of the target center from the road axis (as defined in Sec 4.1, Fig.4.1) is available. Such a measurement can be extracted by image processing techniques, based on high resolution raw image data provided by, e.g, a surveillance camera located on a satellite, helicopter, UAV, etc. This measurement model is given by

$$z_d = d + v_d \tag{63}$$

[4] The time index is dropped in this section for simplicity.

Figure 15: Structure of ME/AME

where the measurement error $v_d \sim \mathcal{N}(0, \sigma_d^2)$ is white noise process.

4.4 Tracking in 1D Road Coordinates using Radar

For 1D (mileage only) tracking it is assumed that the target center is always on the road axis (i.e., the displacement coordinate $d = 0$).

The target motion model, for a state vector $x_k^s = [s_k, \dot{s}_k, \ddot{s}_k]'$, is given by the hybrid system model (52) with known $\boldsymbol{\mu}_0^s$ and Π^s.

Only radar measurements z_r and z_b are available, according to the measurement model given by (58) with $d = 0$.

4.4.1 Mileage Estimator (ME)

The ME implements the IMM filter for the CV-CA multiple model defined by (52) with $M_1^s = CV$ and $M_2^s = CA$. This estimator was proposed and investigated by [[**?**]]. It is considered and implemented here for the purpose of comparison.

4.4.2 Adaptive Mileage Estimator (AME)

The AME implements the IMM filter for the CV-MAA multiple model (52) with $M_1^s = CV$ and $M_2^s = MAA$.

The structure of both estimators is illustrated in Fig.15.

Both ME and AME use extended Kalman filter for conditional filtering (under M_1^s and M_2^s, respectively) since the measurement model (58) with $d = 0$ is nonlinear. The Jacobian

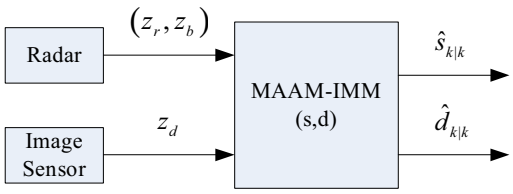

Figure 16: Centralized Estimator

matrix H_k matrix for the EKF is

$$\begin{aligned} H_k &= \left.\frac{\partial h(x^s)}{\partial x^s}\right|_{x^s=\hat{x}^s_{k|k-1},d=0} \\ &= \begin{bmatrix} h_{11}(\hat{s}_{k|k-1},0) & 0 & 0 \\ h_{21}(\hat{s}_{k|k-1},0) & 0 & 0 \end{bmatrix} \end{aligned} \tag{64}$$

where $h_{11}(s,d)$ and $h_{21}(s,d)$ are given by (59) and (60), respectively, and $\hat{s}_{k|k-1}$ is the prediction of a conditional EKF in the IMM .

4.5 Tracking in 2D Road Coordinates using Radar and Image Sensor

In this section we propose three tracking filters in 2D road coordinates using three different schemes for fusion of radar and image-based sensor measurements.

4.5.1 Centralized Estimator (CE)

This estimator, referred to as the *centralized estimator* (CE), is based on the centralized fusion scheme—the measurements from the radar and the image sensor are processed jointly at a fusion center (Fig.16). CE implements the IMM algorithm for the compound multiple model of motion (55)–(57) using both radar and displacement measurements, according to measurement models (58) and (63), respectively. The IMM state vector is $x = [x_k^{s\prime}, d_k]' = [s_k, \dot{s}_k, \ddot{s}_k, d_k]'$ and the filter is based on a total of $2N$ models—two for longitudinal motion (viz., CV-MAA, given by (52) and (51)), each one combined with N models for lateral motion (viz., (53)–(54)). Since the measurement model is nonlinear, extended Kalman filter (EKF) is used for conditional filtering. The Jacobian, based on the coupled measurement

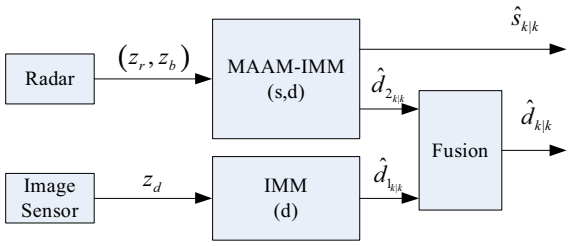

Figure 17: Distributed Estimator

model (58), (63) is as given below.

$$\begin{aligned} H_k &= \left.\frac{\partial h(x)}{\partial x}\right|_{x=\hat{x}_{k|k-1}} \\ &= \left.\begin{bmatrix} h_{11}(s,d) & 0 & 0 & h_{14}(s,d) \\ h_{21}(s,d) & 0 & 0 & h_{24}(s,d) \\ 0 & 0 & 0 & 1 \end{bmatrix}\right|_{\substack{s=\hat{s}_{k|k-1} \\ d=\hat{d}_{k|k-1}}} \end{aligned} \tag{65}$$

where $h_{ij}(s,d)$, $i = 1, 2,\ j = 1, 4$ are given by (59)–(62), and $\hat{x}_{k|k-1}$ is the prediction of a conditional EKF in the IMM.

4.5.2 Distributed Estimator (DE)

This estimator, referred to as the *distributed estimator* (DE), processes the measurements from the radar and the image sensor separately, in a distributed manner as illustrated in Fig.16. DE consists of two IMM filters—IMM(s,d) and IMM(d), and estimate fusion.

Filter IMM(s,d) provides and estimate $\hat{x}_{k|k} = [\hat{x}^{s\prime}_{k|k}, \hat{d}^{(2)}_{k|k}]'$of the state vector $x = [x^{s\prime}_k, d_k]' = [s_k, \dot{s}_k, \ddot{s}_k, d_k]'$. It implements the IMM algorithm for the compound multiple model of motion (55)–(57) using radar measurements according to measurement models (58). The Jacobian, based on the measurement model (58) is as given below.

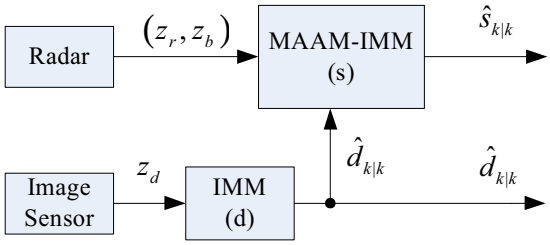

Figure 18: Sequential Estimator

$$\begin{aligned} H_k &= \left.\frac{\partial h(x)}{\partial x}\right|_{x=\hat{x}_{k|k-1}} \\ &= \left.\begin{bmatrix} h_{11}(s,d) & 0 & 0 & h_{14}(s,d) \\ h_{21}(s,d) & 0 & 0 & h_{24}(s,d) \end{bmatrix}\right|_{\substack{s=\hat{s}_{k|k-1} \\ d=\hat{d}^{(2)}_{k|k-1}}} \end{aligned} \tag{66}$$

where $h_{ij}(s,d)$, $i = 1,2,\ j = 1,4$ are given by (59)–(62), and $\hat{x}_{k|k-1}$ is the prediction of a conditional EKF in the IMM(s,d).

Filter IMM(d) implements the IMM algorithm for the latitudinal motion model (53)–(54) with the displacement measurement model (63) and provides an estimate of the displacement, $\hat{d}^{(1)}_{k|k}$. This estimator is referred to as the *lane estimator* (LE) in the sequel.

The estimate fusion provides a fused estimate of the displacement $\hat{d}_{k|k}$ by fusing $\hat{d}^{(1)}_{k|k}$ and$\hat{d}^{(2)}_{k|k}$ at each time-step, according to the following formulas

$$P^{-1}_{\hat{d}_{k|k}} = P^{-1}_{\hat{d}^{(1)}_{k|k}} + P^{-1}_{\hat{d}^{(2)}_{k|k}} \tag{67}$$

$$P^{-1}_{\hat{d}_{k|k}}\,\hat{d}_{k|k} = P^{-1}_{\hat{d}^{(1)}_{k|k}}\,\hat{d}^{(1)}_{k|k} + P^{-1}_{\hat{d}^{(2)}_{k|k}}\,\hat{d}^{(2)}_{k|k} \tag{68}$$

where the variances $P_{\hat{d}^{(1)}_{k|k}} = \mathrm{var}\left(\hat{d}^{(1)}_{k|k}\right)$ and $P_{\hat{d}^{(2)}_{k|k}} = \mathrm{var}\left(\hat{d}^{(2)}_{k|k}\right)$ are provided by IMM(d) and IMM(s,d), respectively, and $P_{\hat{d}_{k|k}} = \mathrm{var}\left(\hat{d}_{k|k}\right)$.

4.5.3 Sequential Estimator (SE)

The structure of this estimator, referred to as the *sequential estimator* (SE), is illustrated in Fig.18. It consists of two IMM filters: IMM(d) and IMM(s).

Filter IMM(d) implements the IMM algorithm for the latitudinal motion model (53)–(54) with the displacement measurement model (63) and provides an estimate of the displacement $\hat{d}_{k|k}$ at each time step k.

Filter IMM(s) provides an estimate of the longitudinal motion (mileage) state vector $\hat{x}^s_{k|k} = [\hat{s}_{k|k}, \hat{\dot{s}}_{k|k}, \hat{\ddot{s}}_{k|k}]'$. It implements the IMM algorithm for the longitudinal CV-MAA motion model (52), (54) with $M^s_2 = MAA$, and the radar measurement model (58) with $d = \hat{d}_{k|k}$ where $\hat{d}_{k|k}$ is provided by IMM(d). Since the measurement model (58) with $d = \hat{d}_{k|k}$ is nonlinear IMM(s) uses EKFs for conditional filtering. The Jacobian matrix H_k matrix for each conditional EKFs is

$$\begin{aligned} H_k &= \left.\frac{\partial h(x^s)}{\partial x^s}\right|_{x^s=\hat{x}^s_{k|k-1}, d=\hat{d}_{k|k}} \\ &= \begin{bmatrix} h_{11}(\hat{s}_{k|k-1}, \hat{d}_{k|k}) & 0 & 0 \\ h_{21}(\hat{s}_{k|k-1}, \hat{d}_{k|k}) & 0 & 0 \end{bmatrix} \end{aligned} \tag{69}$$

where $h_{11}(s,d)$ and $h_{21}(s,d)$ are given by (59) and (60), respectively, $\hat{s}_{k|k-1}$ is the prediction of a conditional EKF in the IMM(s), and $\hat{d}_{k|k-1}$ is the estimate of IMM(d).

SE is a further simplification of the centralized estimator with reduced computational load. Its main idea is to improve the AME (that assumes $d = 0$) via the more accurate approximation $d = \hat{d}_{k|k}$ based on utilizing additional information—the measurements of displacement.

4.6 Simulation and Performance Evaluation

Performance evaluation and comparison of the proposed algorithms were done by Monte-Carlo simulation.

4.6.1 Case 1

4.6.1.1 Scenario

The simulated scenario includes three road segments (Fig.19): a vertical linear segment starting at $(1000m, 0m)$ and ending at $(1000m, 1000m)$, a circular segment with radius of curvature $400m$ and center at $(1400m, 1000m)$, and a horizontal linear segment starting at

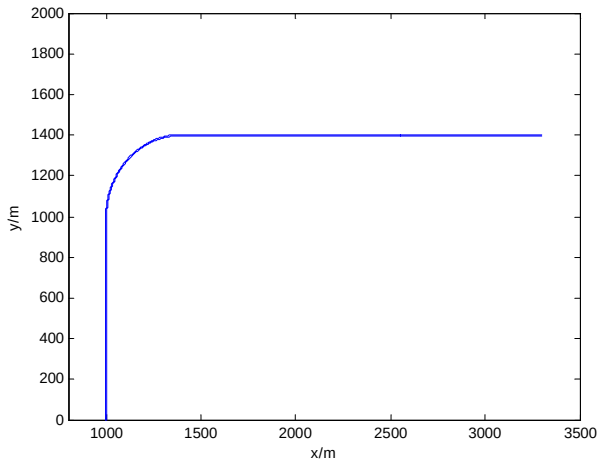

Figure 19: Road Geometry

the end of the circular segment $(1400m, 1400m)$. The number of lanes of the road is $N = 3$, and the width of each lane is $\Delta = 4m$.

The ground truth for the target motion is fixed for both speed changes and lane changes as follows. The target travels along the road, starting at $(1000m, 0m)$. The profiles of the target speed and mileage are shown in Fig.20 and Fig.21, respectively. The target maintains a constant speed of $30m/s$ from the start until approaching the turn segment, then it slows down to $5m/s$, takes the turn with this constant speed, and after leaving the turn it speeds up to $30m/s$ which is then kept constant till the end. The target changes lanes as shown in Fig.23. A process noise $w_k^d \sim \mathcal{N}\left(0, \sigma_{w^d}^2\right)$ with variance $\sigma_{w^d}^2 = 0.3^2 m^2$ is added to the target center displacement (See (53)) which models the deviation from the center of the lane.

The measurements are generated according to the radar and image-based sensor models (58) and (63), respectively. The variances of the measurement errors are $\sigma_r^2 = 4^2 m^2$, $\sigma_b^2 = 0.005^2 rad^2$, and $\sigma_d^2 = 0.8^2 m^2$, respectively. The sampling time period is $T = 1s$.

4.6.1.2 Estimators' Parameters

The variance of process noise of the CV model is $\sigma_{s_{CV}}^2 = 0.01^2 m^2$ for all estimators using this model. The variance of process noise of the CA model is $\sigma_{s_{CA}}^2 = 0.8^2 m^2$ for the mileage estimator ME. For all estimators using the MAA model $\alpha = 1/\tau = 1/15$, and

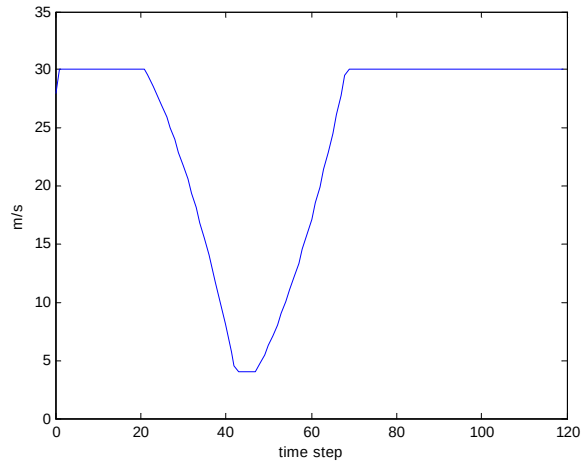

Figure 20: Target Speed Profile

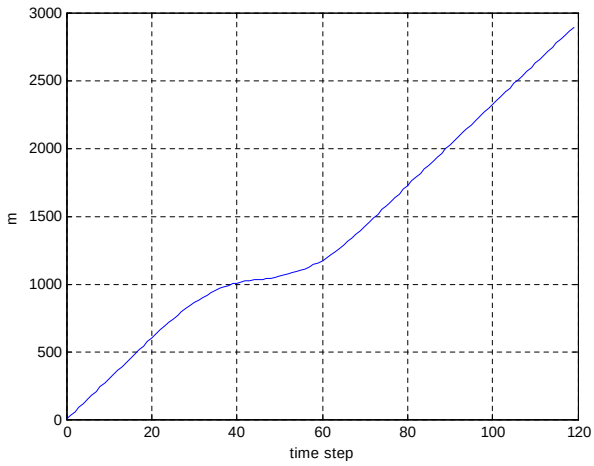

Figure 21: Target Mileage Profile

$a_{\max} = 4.8m/s^2$, $a_{-\max} = -4.8\ m/s^2$.

The variances of the measurement errors used in all estimators are the same as in the ground truth: $\sigma_r^2 = 4^2m^2$, $\sigma_b^2 = 0.005^2rad^2$, and $\sigma_d^2 = 0.8^2m^2$.

The mileage estimators ME/AME and the sequential estimator SE use the initial probability vector $\boldsymbol{\mu}_0^s = [0.5, 0.5]'$ and the transition probability matrix

$$\Pi^s = [\pi_{ij}^s]_{i,j=1}^2 = \begin{bmatrix} 0.95 & 0.05 \\ 0.05 & 0.95 \end{bmatrix}$$

The lane estimator IMM(d) uses the initial probability vector $\boldsymbol{\mu}_0^d = [0.3, 0.4, 0.3]'$ and the transition probability matrix

$$\Pi^d = [\pi_{ij}^d]_{i,j=1}^3 = \begin{bmatrix} 0.97 & 0.028 & 0.002 \\ 0.015 & 0.97 & 0.015 \\ 0.002 & 0.028 & 0.97 \end{bmatrix}$$

The centralized estimator CE and IMM(s,d) in the distributed estimator DE use six models, enumerated as M_j for $j = 1, 2, ..., 6$, where $j = 1, 2, 3$ stands for CV model and lane j, respectively, and $j = 4, 5, 6$ stands for MAA model and lane $(j - 3)$, respectively. The initial probability vector $\boldsymbol{\mu}_0 = [0.15, 0.2, 0.15, 0.15, 0.2, 0.15]'$, and the transition probability matrix $\Pi = [\pi_{ij}]_{i,j=1}^6$ is

$$\begin{bmatrix} 0.95 & 0.016 & 0.004 & 0.025 & 0.004 & 0.001 \\ 0.01 & 0.95 & 0.01 & 0.0025 & 0.025 & 0.0025 \\ 0.004 & 0.016 & 0.95 & 0.001 & 0.004 & 0.025 \\ 0.025 & 0.004 & 0.001 & 0.95 & 0.016 & 0.004 \\ 0.0025 & 0.025 & 0.0025 & 0.01 & 0.95 & 0.01 \\ 0.001 & 0.004 & 0.025 & 0.004 & 0.016 & 0.95 \end{bmatrix}$$

4.6.1.3 Results

All results are based on 200 Monte Carlo runs.

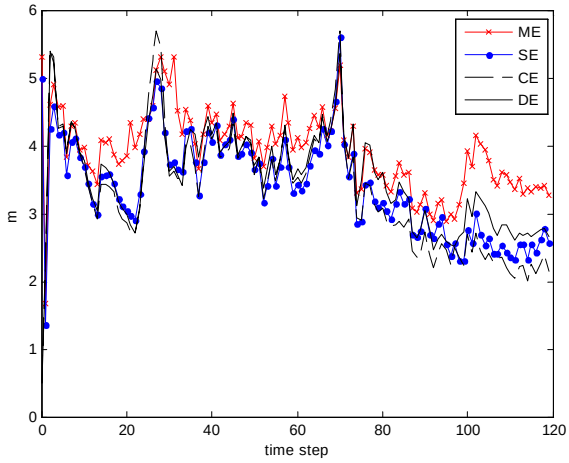

Figure 22: RMS Errors for Mileage-OnlyTracking

First, we compare the proposed estimators CE, DE and SE for mileage only tracking with the mileage estimator ME proposed previously in [**2**]. Fig.22 shows the RMS errors of the mileage state estimates $\hat{x}^s_{k|k}$ of the four algorithms. Clearly, all three proposed estimators outperform the existing ME. Apparently, for CE and SE this improvement can be explained partially by the fact that they use more data—the additional displacement measurement. However, DE uses the same (radar only) measurements as ME for estimating the mileage state, and DE is still considerably better than ME. This improvement can be explained by the fact that DE uses the MAA model for longitudinal maneuvering while ME uses the CA model. This is the only difference between these two estimators which indicates that using the MAA model is better for longitudinal maneuvers than the CA model.

Next, we investigate the performance of the proposed estimators.

Fig.23 shows both the ground truth of lateral motion (lane changing) and the average estimated target location (in terms of displacement coordinate only) based on the lane estimator IMM(d), as an independent part of DE and SE. Fig.24 shows the IMM probabilities. The position estimates and lane identification capabilities of IMM(d) are very good in this case because the process and measurement noises are quite small. As this noises increase (shown later) this estimation/identification performance degrades considerably.

Fig.25 compares the RMS error of the three lane estimates in DE: $\hat{d}^{(1)}_{k|k}$ produced by

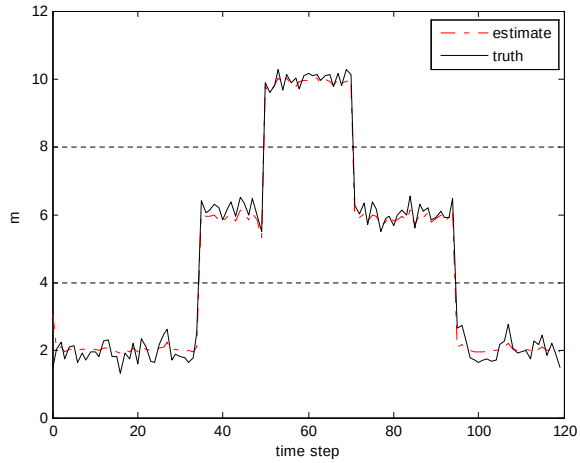

Figure 23: Lane Estimator IMM(d): True & Estimated States

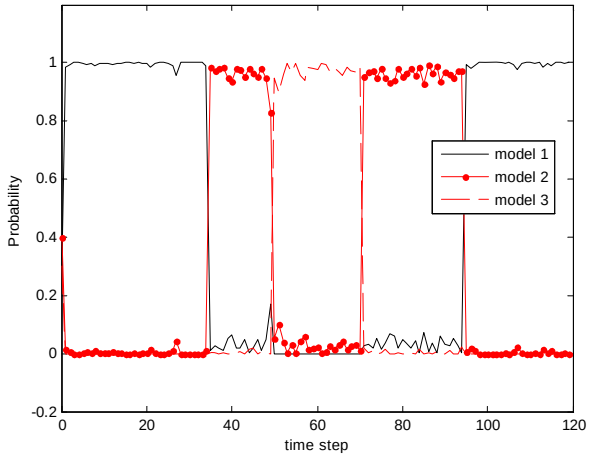

Figure 24: Lane Estimator IMM(d): IMM Probabilities

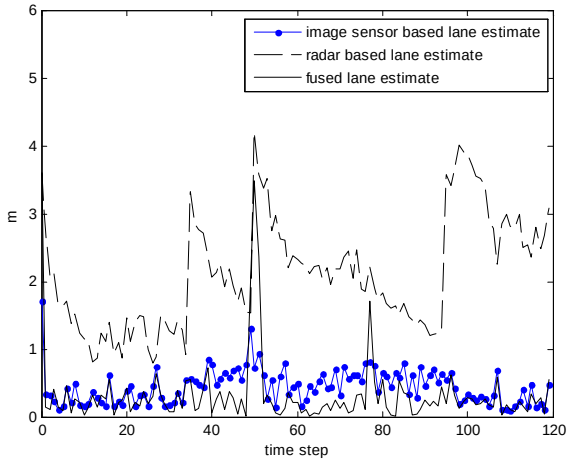

Figure 25: RMSE of Lane Estimation in DE

IMM(d), $\hat{d}^{(2)}_{k|k}$ produced by the radar IMM(s,d), and the fused estimate $\hat{d}_{k|k}$ produced by (67)–(68). The image-sensor based estimate $\hat{d}^{(1)}_{k|k}$ is significantly more accurate than radar based estimate $\hat{d}^{(2)}_{k|k}$. Despite the better accuracy of the image-based direct measurements of d as compared to the radar measurements, this is also due to the fact that the radar measurement model of IMM(s,d) is highly nonlinear and the locally linear approximation used by the EKF appears to be rather crude. More importantly, Fig.25 illustrates that the fused estimate $\hat{d}_{k|k}$ is considerably better than both local estimates $\hat{d}^{(1)}_{k|k}$ and $\hat{d}^{(2)}_{k|k}$. This result was consistently confirmed in all our simulations.

Fig.26 compares the RMS errors of lane estimation of CE, DE and SE. SE appears to be slightly worse than CE and DE which are close themselves. This can be explained by the fact that SE actually ignores the information about d which is contained in the radar measurements—it only uses the information about d provided by the image-sensor based measurements. Somewhat surprisingly, the distributed estimator DE has about the same accuracy (even better, sometimes) as the fully coupled centralized estimator DE. There is no theoretical contradiction here because the estimation problem is highly nonlinear and both algorithms are very approximate.

The overall position RMS errors in global Cartesian coordinates (obtained by converting the errors in $\hat{x}^s$ and $\hat{d}$ to Cartesian coordinates) are shown in Fig.27. The CE appears slightly

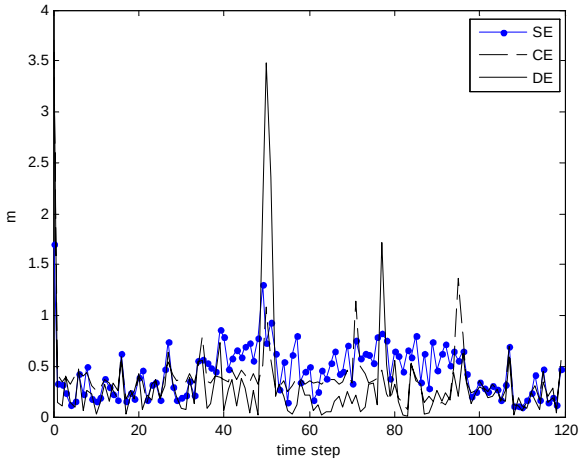

Figure 26: RMSEs of Lane Estimation of CE, DE, and SE

better than DE and SE but the differences for this scenario are minor.

In order to illustrate the target motion mode identification capabilities of CE and DE, Fig.28 and Fig.29 show the model probability of CE and DE, respectively. In both figures the model probabilities change reasonably well when the target performs longitudinal and lateral maneuvers (lane changing) but, overall, the model probability of CE in Fig.28 are better than that of DE in Fig.29. The reason for this is that CE it uses measurements from both radar and image sensor while the IMM(s,d) filter of DE uses only radar measurements.

When judging on the overall performance of CE, DE and SE it should be kept in mind that DE requires much less computation than CE, and, furthermore, SE requires less computation than DE. (The comparative execution times of the three algorithms will be provided in the final version).

Next we present simulation results from another scenario.

4.6.2 Case 2

4.6.2.1 Senario and Estimators' Parameters

In this scenario, a process noise $w_k^d \sim \mathcal{N}\left(0, \sigma_{w^d}^2\right)$ with variance $\sigma_{w^d}^2 = 0.4^2 m^2$ is added to the target center displacement which models the deviation from the center of the lane. The variance of the measurement error in image sensor is $\sigma_d^2 = 1.0^2 m^2$. Fig.31 shows both the

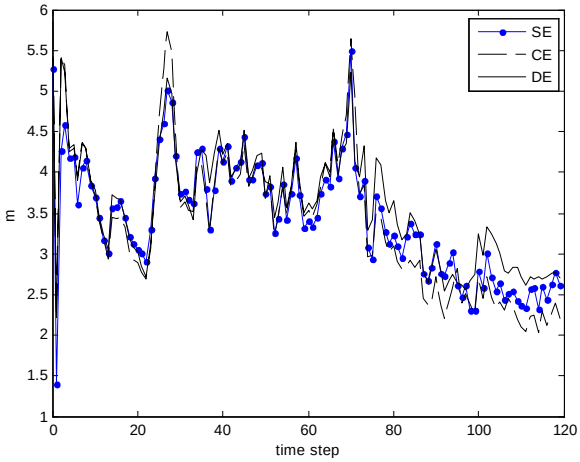

Figure 27: Overall Position RMSEs in Cartesian Coordinates

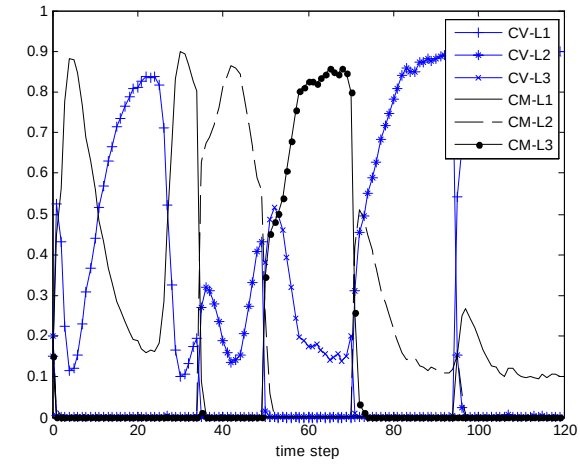

Figure 28: Model Probabilities of CE

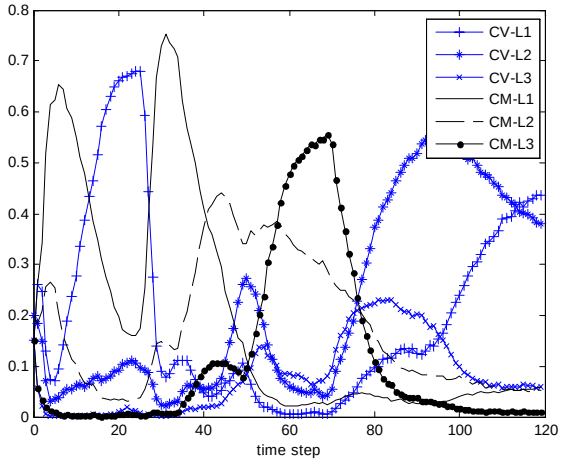

Figure 29: Model Probabilities of DE

ground truth of lateral motion (lane changing) and the average estimated target location (in terms of displacement coordinate only) based on the lane estimator IMM(d). For estimators' parameters, the variance of the measurement error from image sensor used in all estimators is the same as in the ground truth: $\sigma_d^2 = 1.0^2 m^2$. Other parameters in this senario and the estimators are the same as that given in the above simulation.

4.6.2.2 Results

All results are based on 200 Monte-Carlo runs.

Fig.30 shows the RMS errors of the mileage state estimates $\hat{x}^s_{k|k}$ of the four algorithms. With larger measurement errors from image sensor, it is obvious that all three proposed estimators outperform the existing ME. Based on measurement only from radar, DE is still considerably better than ME. This improvement is still obvious by using the MAA model for longitudinal maneuvering.

Fig.31 shows both the ground truth of lateral motion (lane changing) and the average estimated target location (in terms of displacement coordinate only). Fig.32 shows the IMM probabilities. We can see that this estimation/identification performance of the position estimates and lane identification capabilities of IMM(d) degrades considerably as the noises increase.

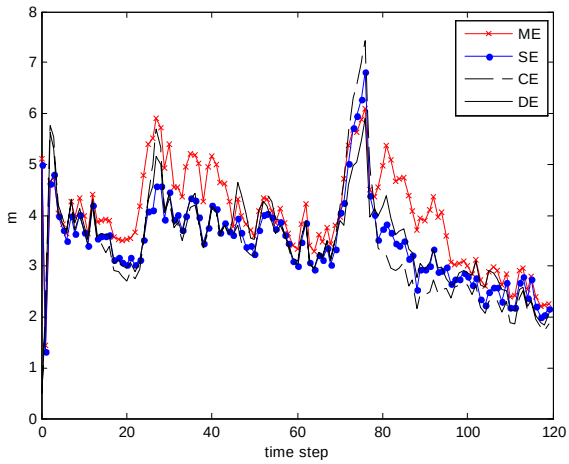

Figure 30: The RMS error of mileage estimate of four approaches

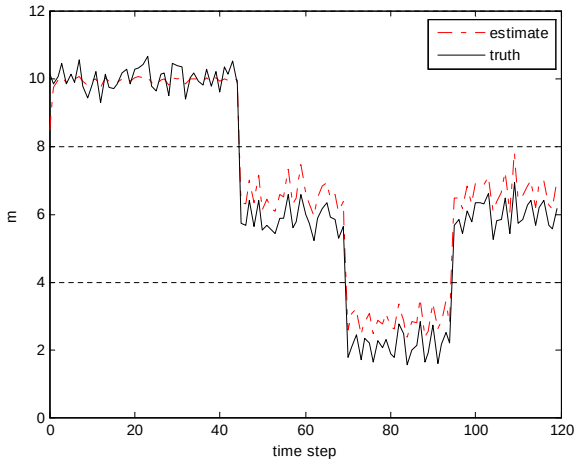

Figure 31: True states and average lane estimate

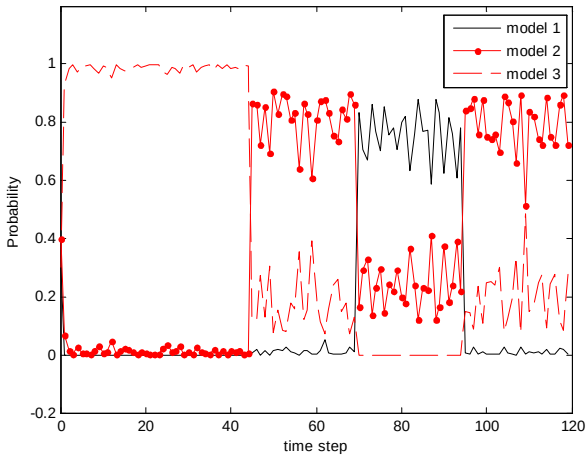

Figure 32: The model probability of lane estimator

Fig.33 compares the RMS error of the three lane estimates in DE: $\hat{d}^{(1)}_{k|k}$ produced by IMM(d), $\hat{d}^{(2)}_{k|k}$ produced by the radar IMM(s,d), and the fused estimate $\hat{d}_{k|k}$. Fig.33 illustrates that with larger measurement error, the fused estimate $\hat{d}_{k|k}$ is considerably better than both local estimates $\hat{d}^{(1)}_{k|k}$ and $\hat{d}^{(2)}_{k|k}$.

Fig.34 compares the RMS errors of lane estimation of CE, DE and SE. Clearly, SE appears to be worse than CE and DE which are close themselves. The reason is that with large observation errors from image sensor, the estimation/identification performance of the position estimates and lane identification capabilities of IMM(d) degrades considerably when lane changes.

The overall position RMS errors in global Cartesian coordinates (obtained by converting the errors in $\hat{x}^s$ and $\hat{d}$ to Cartesian coordinates) are shown in Fig.35. The CE still appears slightly better than DE and SE but the differences for this scenario are minor.

Fig.36 and Fig.37 show the model probability of CE and DE, respectively to illustrate the target motion mode identification capabilities of CE and DE. With larger measurement errors from image sensor, in both figures the model probabilities change reasonably well when the target performs longitudinal and lateral maneuvers (lane changing) but, overall, the model probability of CE in Fig.36 are still better than that of DE in Fig.37.

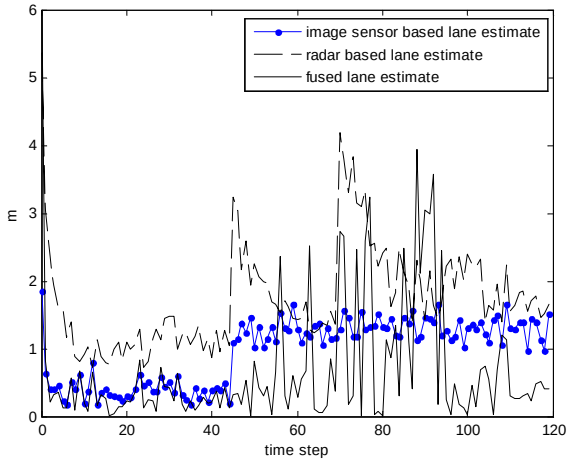

Figure 33: RMSE of Lane Estimation in DE

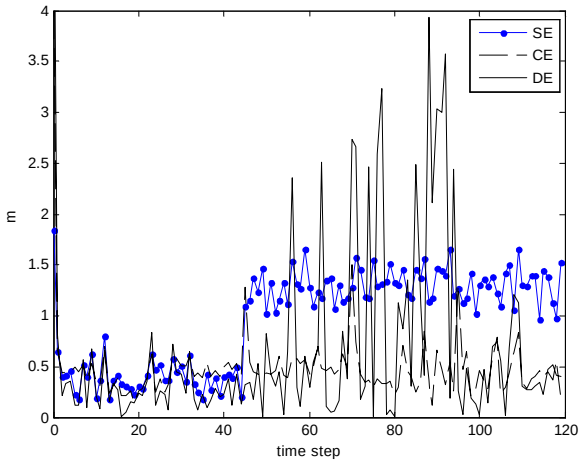

Figure 34: The RMS error of lane estimate of three approaches

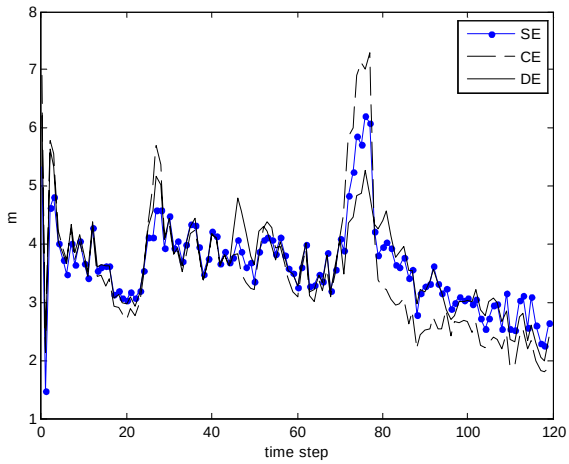

Figure 35: The RMS error of fusion of mileage and lane estimates of three approaches

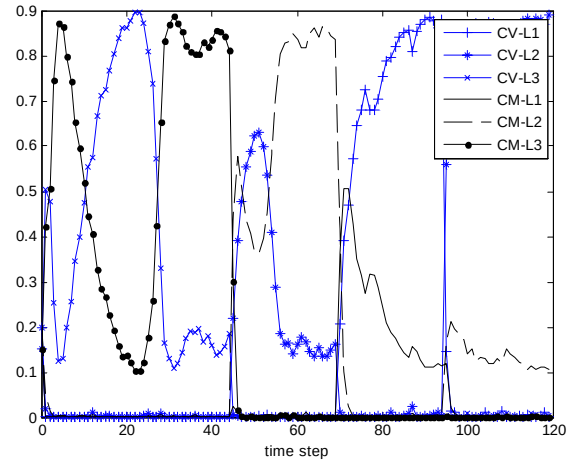

Figure 36: The model probability of CE

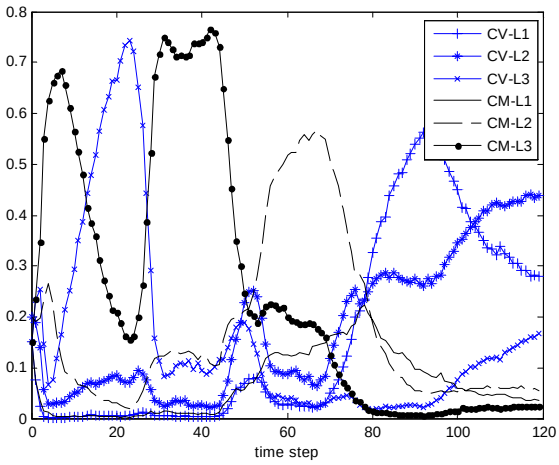

Figure 37: The model probability of DE

CHAPTER V

CONCLUSIONS

We use the HMM framework to formulate and solve the lane tracking problem. The *lane sequence estimator* (LSE) is formulated in terms of the optimal estimation of the lane sequence and the *lane filter* (LF) is formulated in terms of the optimal estimation of the current lane of the target, given the observations from the start time to the current time.

From the simulation and analysis we can see that the implemented algorithms, viz., the LSE and LF, provide reasonable performance for the lane tracking problem. After 50 time steps the average probability of correct estimation of the LSE is around 0.92 which is much larger than the probability of correct observation in the observation probability matrix. The probability of being correct at the current time of the LF is also much larger than the probability of correct observation in the observation probability matrix. To estimate the lane sequence, the LSE is better than the LF. To identify the lane at the current time, the LF is better than the LSE. The two algorithms can effectively identify the lane which an on-road target is in. It has been established in the simulation that the choice of lane TPM affects the lane tracking performance heavily. Identifying the lane transition probability matrix is an important problem for further work.

A novel 2D road coordinate representation of an on-road moving target has been proposed. It is very convenient in modeling longitudinal and lateral vehicle motions for target tracking. A natural description of target maneuvering behavior in 2D road coordinates has been given using multiple models. Three estimators have been developed by using different schemes for fusion of radar and image-based measurement data: centralized (CE), distributed (DE), and sequential (SE).

The simulation results have demonstrated that

- All proposed algorithms (CE, DE and SE) significantly outperform the known ME for mileage tracking.

- The proposed mean adaptive acceleration (MAA) model is better than the nearly constant acceleration (CA) model for describing longitudinal maneuver modes of motion.
- The estimate-based fusion in DE for displacement estimation is effective—it improves both local estimates consistently.
- The estimation/identification performance of the position estimates and lane identification capabilities of IMM(d) degrades considerably as the measurement noises of image sensor increase.
- Overall, CE is slightly more accurate than the simplified versions DE and CE, however, they have considerably reduced computational load.

REFERENCES

[1] Chen, Yangsheng, Li, X. Rong and Jilkov, Vesselin. Lane Tracking for On-Road Targets. In *Proc. 2008 International Conf. on Information Fusion,* Cologne, Germany, July 2008.

[2] Chen, Yangsheng, Li, X. Rong and Jilkov, Vesselin. On-Road Target Tracking using Radar and Image Sensor Based Measurements. Submitted to *2009 International Conf. on Information Fusion*

[3] Li, X. R., and Jilkov, V. P. Survey of Maneuvering Target Tracking-Part I: Dynamic Models. *IEEE Transactions on Aerospace and Electronic Systems*, 39:1333-1364, 2003.

[4] T. Kirubarajan, Y. Bar-Shalom, K. Pattipati, and I. Kadar. Ground Target Tracking with a GMTI Structure IMM Estimator. *IEEE Transactions on Aerospace and Electronic Systems*, 36(1):26–46, Jan. 2000.

[5] Ke, C.-C., Herrero, J. G. and Llinas J. Comparative Analysis of Ground Target Tracking Techniques. In *Proc. 2000 International Conf. on Information Fusion*, pages WeB5–1, Paris, France, July 2000.

[6] Mallick, M. and Arulampalam, S. Comparative of Nonlinear Filtering Algorithms in Ground Moving Target Indicator (GMTI) Target Tracking. In *Proc. Signal and Data Processing of Small Targets*, San Diego, CA, Aug. 2003.

[7] Kirubarajan, T. and Bar-Shalom, Y. Tracking Evasive Move-Stop-Move Tarets with a GMTI Radar Using a VS-IMM Estimator. *IEEE Trans. Aerospace and Electronic Systems*, 39(3):1098–1103, 2003.

[8] Farina, A., Ferranti, L. and Golino, G. Constrained Tracking Filters for A-SMGCS. In *Proc. 2003 International Conf. on Information Fusion*, pages 414–421, Cairns, Australia, July 2003.

[9] Kastella, K. and Kreucher, C. Multiple Model Nonlinear Filtering for Low Signal Ground Target Applications. *IEEE Trans. Aerospace and Electronic Systems*, 41(2):549–564, Apr. 2005.

[10] Benameur, K., Pannetier, B. and Nimier, V. A Comparative Study on the Use of Road Network Information in GMTI Tracking. In *Proc. 2005 International Conf. on Information Fusion*, Philadelphia, PA, USA, July 2005.

[11] Yang, C., Bakich, M. and Blasch, E. P. Nonlinear Constrained Tracking of Targets on Roads. In *Proc. 2005 International Conf. on Information Fusion*, Philadelphia, PA, USA, July 2005.

[12] Ulmke, M. and Koch, W. Road-Map Assisted Ground Moving Target Tracking. *IEEE Transactions on Aerospace and Electronic Systems*, 42(4):1264–1274, Oct. 2006.

[13] Ekman, M and Sviestins, E. Multiple Model Algorithm Based on Particle Filters for Ground Target Tracking. In *Proc. 2003 International Conf. on Information Fusion*, 2007.

[14] Streller, D. Road Map Assisted Ground Target Tracking. In *Proc. 2003 International Conf. on Information Fusion*, 1162–1168, 2008.

[15] Layne, J., and Eilders, M.J., A Prediction and Search Algorithm Using Fuzzy Dynamic Models, Air Force Technology Horizon, 2004.

[16] Kirubarajan, T. and Bar-Sharlom, Y. Ground Target Tracking with Variable Structure IMM Estimator. *IEEE T-AES*, 36, 2000.

[17] Shea, P.J. and Klamer, D. Use of Roads for Improved Tracking of Moving Ground Targets. *Fourth ONR/GTRI Workshop on Target Tracking & Sensor Fusion*, 2001.

[18] Yang, C. Hybrid Unscented Kalman Particle Filter for Ground Target Tracking. Interim Report, No. 3, 2004.

[19] Rabiner, L. R. and Juang, B. H. An Introduction to Hidden Markov Models. *IEEE ASSP Mag.*, 4-6, Jun. 1986.

[20] Dugad, R. and Desai, U. B. A Tutorial on Hidden Markov Models. URL: http://citeseer.ist.psu.edu/dugad96tutorial.html

[21] Elliott, R. J., Aggoun, L. and Moore, J. B. Hidden Markov Models, Estimation and Control. New York: Springer-Verlag, 1995.

[22] Raviv, J. Decision Making in Markov Chains Applied to the Problem of Pattern Recognition. *IEEE Trans. Inf. Theory*, IT-13(4):536-551, 1967.

[23] Ephraim, Y. and Merhav, N. Hidden Markov Processes. *IEEE Trans. Inf. Theory*, 48(6):1518-1569, Jun 2002.

[24] Bridle, J. S. Stochastic Models and Template Matching: Some Important Relationships Between two Apparently Different Techniques for Automatic Speech Recognition. In *Proc. Inst. Of Acoustics, Autum Conf.*, 1-8, Nov 1984.

[25] Rabiner, L. R. A Tutorial on Hidden Markov Models and Selected Applications in Speech Recognition. *Proceedings of IEEE*, 77(2):257-286, 1989.

[26] Obermaier, B., Guger, C. and Pfurtscheller, G. HMM Used for the Offline Classification of EEG Data. *Biomedizinsche Technik*, June 1999.

[27] http://en.wikipedia.org/wiki/Regular_parametric_curve#Definitions

VITA

The author was born in Huaining, Anhui Province, China in 1980. He received a B.S in Electric Engineering and Automation in 2003 from Changsha Institute of Technology. From 2006 to 2009, he worked as research assistant at University of New Orleans. The author's research interests include statistical signal processing, signal processing in communication, target tracking, statistics and stochastic control.